Article

RNA neoantigen vaccines prime long-lived CD8$^+$ T cells in pancreatic cancer

https://doi.org/10.1038/s41586-024-08508-4

Received: 5 April 2024

Accepted: 10 December 2024

Published online: 19 February 2025

Open access

Check for updates

Zachary Sethna[1,2,3,4,14], Pablo Guasp[1,2,14], Charlotte Reiche[1,2], Martina Milighetti[1,2,4], Nicholas Ceglia[4], Erin Patterson[3], Jayon Lihm[3,4], George Payne[1,2], Olga Lyudovyk[4], Luis A. Rojas[1,2], Nan Pang[2], Akihiro Ohmoto[1,2], Masataka Amisaki[1,2], Abderezak Zebboudj[1,2], Zagaa Odgerel[1,2], Emmanuel M. Bruno[1,2], Siqi Linsey Zhang[1,2], Charlotte Cheng[1,2], Yuval Elhanati[4], Evelyna Derhovanessian[5], Luisa Manning[5], Felicitas Müller[5], Ina Rhee[6], Mahesh Yadav[6], Taha Merghoub[7], Jedd D. Wolchok[7], Olca Basturk[8], Mithat Gönen[9], Andrew S. Epstein[10], Parisa Momtaz[10], Wungki Park[10,11], Ryan Sugarman[10], Anna M. Varghese[10], Elizabeth Won[10], Avni Desai[10], Alice C. Wei[2,11], Michael I. D'Angelica[2,11], T. Peter Kingham[2,11], Kevin C. Soares[2,11], William R. Jarnagin[2,11], Jeffrey Drebin[2,11], Eileen M. O'Reilly[10,11], Ira Mellman[6], Ugur Sahin[5,12], Özlem Türeci[5,12], Benjamin D. Greenbaum[3,4,13,15] & Vinod P. Balachandran[1,2,3,11,15] ✉

A fundamental challenge for cancer vaccines is to generate long-lived functional T cells that are specific for tumour antigens. Here we find that mRNA–lipoplex vaccines against somatic mutation-derived neoantigens may solve this challenge in pancreatic ductal adenocarcinoma (PDAC), a lethal cancer with few mutations. At an extended 3.2-year median follow-up from a phase 1 trial of surgery, atezolizumab (PD-L1 inhibitory antibody), autogene cevumeran[1] (individualized neoantigen vaccine with backbone-optimized uridine mRNA–lipoplex nanoparticles) and modified (m) FOLFIRINOX (chemotherapy) in patients with PDAC, we find that responders with vaccine-induced T cells ($n = 8$) have prolonged recurrence-free survival (RFS; median not reached) compared with non-responders without vaccine-induced T cells ($n = 8$; median RFS 13.4 months; $P = 0.007$). In responders, autogene cevumeran induces CD8$^+$ T cell clones with an average estimated lifespan of 7.7 years (range 1.5 to roughly 100 years), with approximately 20% of clones having latent multi-decade lifespans that may outlive hosts. Eighty-six percent of clones per patient persist at substantial frequencies approximately 3 years post-vaccination, including clones with high avidity to PDAC neoepitopes. Using PhenoTrack, a novel computational strategy to trace single T cell phenotypes, we uncover that vaccine-induced clones are undetectable in pre-vaccination tissues, and assume a cytotoxic, tissue-resident memory-like T cell state up to three years post-vaccination with preserved neoantigen-specific effector function. Two responders recurred and evidenced fewer vaccine-induced T cells. Furthermore, recurrent PDACs were pruned of vaccine-targeted cancer clones. Thus, in PDAC, autogene cevumeran induces de novo CD8$^+$ T cells with multiyear longevity, substantial magnitude and durable effector functions that may delay PDAC recurrence. Adjuvant mRNA–lipoplex neoantigen vaccines may thus solve a pivotal obstacle for cancer vaccination.

We previously reported[1] early clinical and immunologic results of an investigator-initiated, phase 1 trial of adjuvant sequential anti-PD-L1 (atezolizumab, single pre-vaccination dose), followed by 8 intravenous priming doses of an individualized uridine-based mRNA neoantigen vaccine (autogene cevumeran; containing up to 20 major histocompatibility complex class I (MHCI) and class II (MHCII) restricted neoantigens against predominantly somatic passenger mutations administered 3 weeks after atezolizumab), mFOLFIRINOX (12 cycles) and a single vaccine boost dose (Extended Data Fig. 1a) in 19 patients with surgically resected PDAC (the safety-evaluable cohort comprised 16 vaccinated patients and 3 atezolizumab-treated patients). At a median follow-up of 1.5 years, in 8 out of the 16 vaccinated patients (biomarker-evaluable cohort), autogene cevumeran induced high-magnitude, polyfunctional neoantigen-specific CD8$^+$ effector T cells that correlated with delayed PDAC recurrence[1]. Here we double the clinical and immunologic follow-up time to probe whether vaccine-induced CD8$^+$ T cells: (1) durably correlate with delayed PDAC recurrence; (2) persist long term as putative memory T cells; and (3) retain effector function long term.

A list of affiliations appears at the end of the paper.

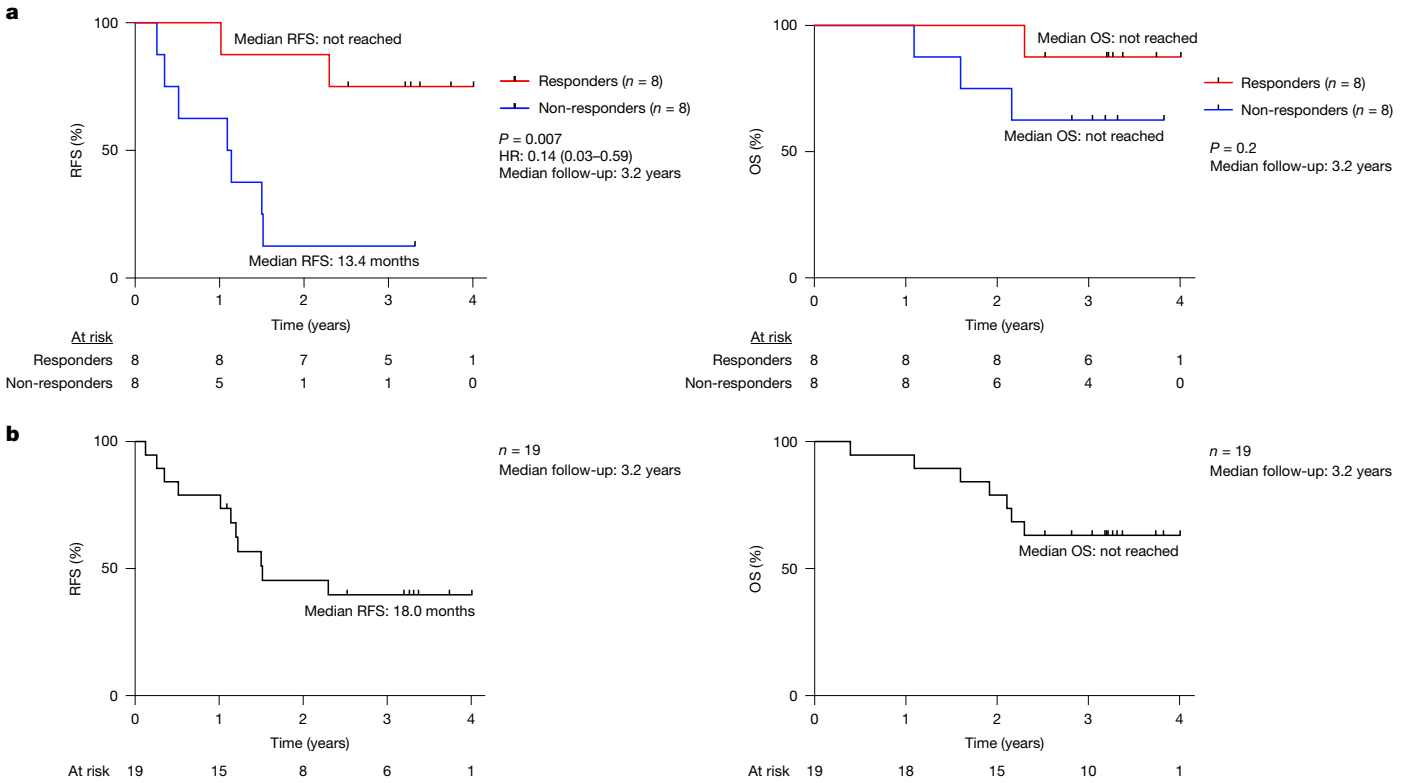

Fig. 1 | mRNA vaccine immune response correlates with delayed PDAC recurrence at three-year follow-up. a, RFS and OS stratified by vaccine response in the biomarker-evaluable cohort. **b**, RFS and OS in the safety-evaluable cohort. HR, hazard ratio, with 95% confidence interval. Black tick marks indicate censorship points. *n* is the number of individual patients; *P* values by two-tailed log-rank test. Numbers of at-risk patients are shown below the graphs.

Clinical outcome at extended follow-up

In the biomarker-evaluable cohort[1], at a median follow-up of 3.2 years (range 2.3–4.0 years), the 8 patients with vaccine-induced high-magnitude neoantigen-specific T cells determined by ex vivo IFNγ ELISpot[1] (responders) had a median RFS that was not reached (Fig. 1a, left). By contrast, the 8 patients without vaccine-induced T cells (non-responders) had a median RFS of 13.4 months (P = 0.007; hazard ratio = 0.14, 95% confidence interval 0.03–0.59; Fig. 1a, left). The effect size between vaccine responders and non-responders was similar to the observed effect size at 1.5-year median follow-up[1], including by landmark analysis to exclude a time-to-response bias (Extended Data Fig. 1b, left). Consistent with our previous findings that vaccine responders were not merely enriched in patients responding to atezolizumab or patients with better prognosis[1], atezolizumab immune response (Methods) and tumour size did not correlate with delayed recurrence (Extended Data Fig. 1b, middle and right). We previously reported[1] equivalent clinicopathologic prognostic features and comparable immune competence throughout the study period in responders and non-responders, with similar humoral and cellular immunity to concurrent unrelated mRNA vaccination (SARS-CoV-2). Median overall survival (OS) was not reached in responders or non-responders (Fig. 1a, right) at extended follow-up. In the safety-evaluable cohort, the median RFS was 18.0 months, and median OS was not reached (Fig. 1b). Thus, autogene cevumeran response may durably correlate with delayed PDAC recurrence.

Vaccines elicit long-lived T cell clones

To investigate whether vaccine-induced T cells persist, we traced the origin and longevity of vaccine-induced T cell clones in all responders (Fig. 2a). To do so, we applied CloneTrack[1], which utilizes T cell receptor (TCR) Vβ sequencing of peripheral blood before and after vaccination to detect and trace high-magnitude vaccine-induced T cell clones (Methods). We previously reported[1] that in responders, CloneTrack-identified clones are nearly all $CD8^+$ T cells and include $CD8^+$ T cells specific to the subset of vaccine neoantigens that trigger positive ex vivo IFNγ ELISpot responses post-priming (25 of 108 vaccine neoantigens in 8 responders were ELISpot-positive[1]; Fig. 2b, top).

Applying CloneTrack from pre-vaccination to approximately 4 years post-vaccination (5.47 million clones, 9.95 million cells in 131 samples across 26 timepoints; Fig. 2a) across all 8 responders, we identify that vaccines induce 79 T cell clones post-priming ('CloneTrack clones'; Fig. 2b, top) with multiple clones in all patients (Extended Data Fig. 2a) and no new boost-induced clones in the 7 responders who received a boost dose (Fig. 2b, bottom and Extended Data Fig. 2b). By mapping cognate clones to all 25 ELISpot-positive vaccine neoantigens, we find that 29 out of 79 (37%) CloneTrack clones in 7 out of 8 responders are ELISpot-positive vaccine neoantigen-specific $CD8^+$ T cells (Fig. 2b, bottom and Extended Data Fig. 3a–c; the remaining 50 CloneTrack clones were unmapped), including 15 clones in 5 responders with confirmed specificity to vaccine neoantigens by TCR cloning and minimal neoepitope mapping (Extended Data Fig. 3a–c). Although CloneTrack clones peaked with variable numbers of vaccine doses (Extended Data Fig. 4a) to different magnitudes (Extended Data Fig. 4b), 77% of CloneTrack clones reached peak expansion with 6 or fewer priming doses (Extended Data Fig. 4a), with individual clones expanding approximately 100-fold or more (Extended Data Fig. 4c) to a median peak percentage of 0.2% of all peripheral T cells (Extended Data Fig. 4d, top). Thus, in patients with PDAC, autogene cevumeran priming doses, but not boost, induce high-magnitude T cell clones.

Next, to examine whether CloneTrack clones can persist long term despite patients receiving mFOLFIRINOX immediately after priming

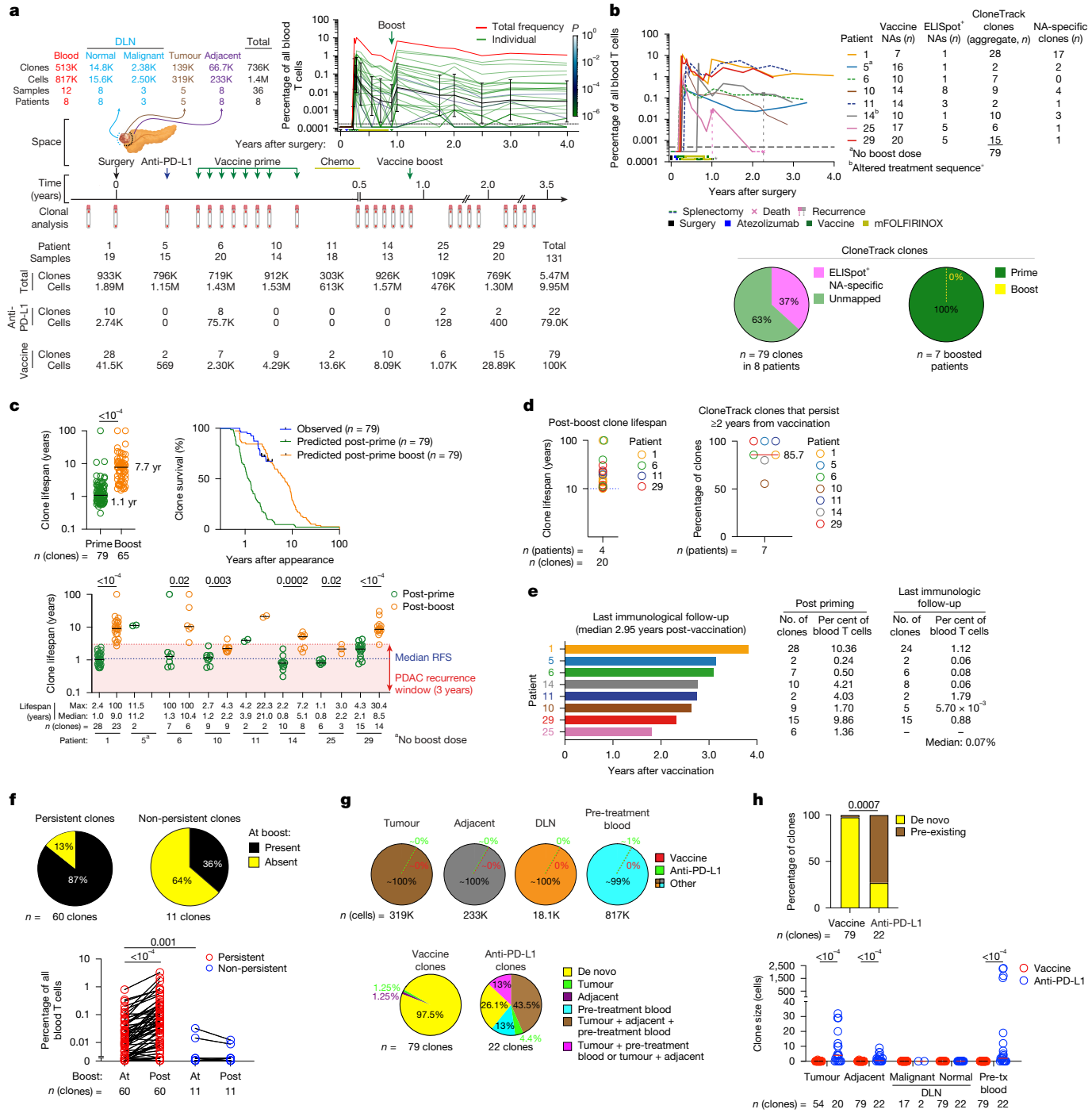

Fig. 2 | mRNA vaccines induce T cells with multiyear lifespans de novo. **a**, Analysed T cell clones in tissues and blood. Total includes all blood T cells and clones; anti-PD-L1 and vaccine clones identified by CloneTrack. Top right, trajectory of T cell clones from patient 1. Anti-PD-L1, atezolizumab; chemo, mFOLFIRINOX; vaccine prime and boost doses, autogene cevumeran. **b**, Top left, longitudinal aggregate percentage of vaccine-induced clones in responders. Coloured rectangles indicate times of surgery, atezolizumab, vaccination and mFOLFIRINOX; asterisk (*) indicates the altered treatment sequence for patient 14. The horizontal dashed line shows the threshold for clone detection. Top right, number of neoantigens (NAs) with validated neoantigen-specific clones. Bottom, percentage of clones mapped to ELISpot-positive (ELISpot$^+$) neoantigens (left) and induced by vaccine prime and boost doses (right). **c**, Estimated clone lifespan in all (top left) and individual (bottom) patients. Bottom, the red shaded region indicates the three-year historical PDAC recurrence window; median RFS is the historical post-surgery PDAC RFS. Top right, observed versus estimated clone survival. No boost lifespans are shown for 14 clones owing to absent boost or clones. **d**, Left, top clone lifespans in four patients with highest-longevity clones. The dotted line indicates ten years post-vaccination. Right, percentage of clones per patient that persist two years or more post-vaccination (persistent clones). Patient 25 died less than 2 years post-vaccination. **e**, Last immunologic follow-up (left; median 2.95 years post-vaccination) and number and aggregate percentage of clones post-priming (all patients) and at last follow-up (patients with persistent clones) (right). **f**, Percentage of persistent and non-persistent clones at boost in $n = 6$ boosted patients among clones (top) and among all blood T cells (bottom). **g**, Top, percentage of tissue T cells containing treatment clones. Bottom, percentage of treatment clones contained in tissues. n is the number of tissue T cells (top) and treatment-induced clones (bottom). **h**, Percentage of treatment clones in peripheral blood present (pre-existing) or absent (de novo) in tissues pre-treatment (top) and associated clone sizes (bottom). All treatment-induced clones were identified by CloneTrack. Pre-tx, pre-treatment. n is the number of clones, cells or patients. P values by two-tailed Mann–Whitney test (**c**, **h**, bottom), two-tailed Wilcoxon matched-pairs signed rank test (**f**, bottom) and two-sided chi-squared test (**h**, top).

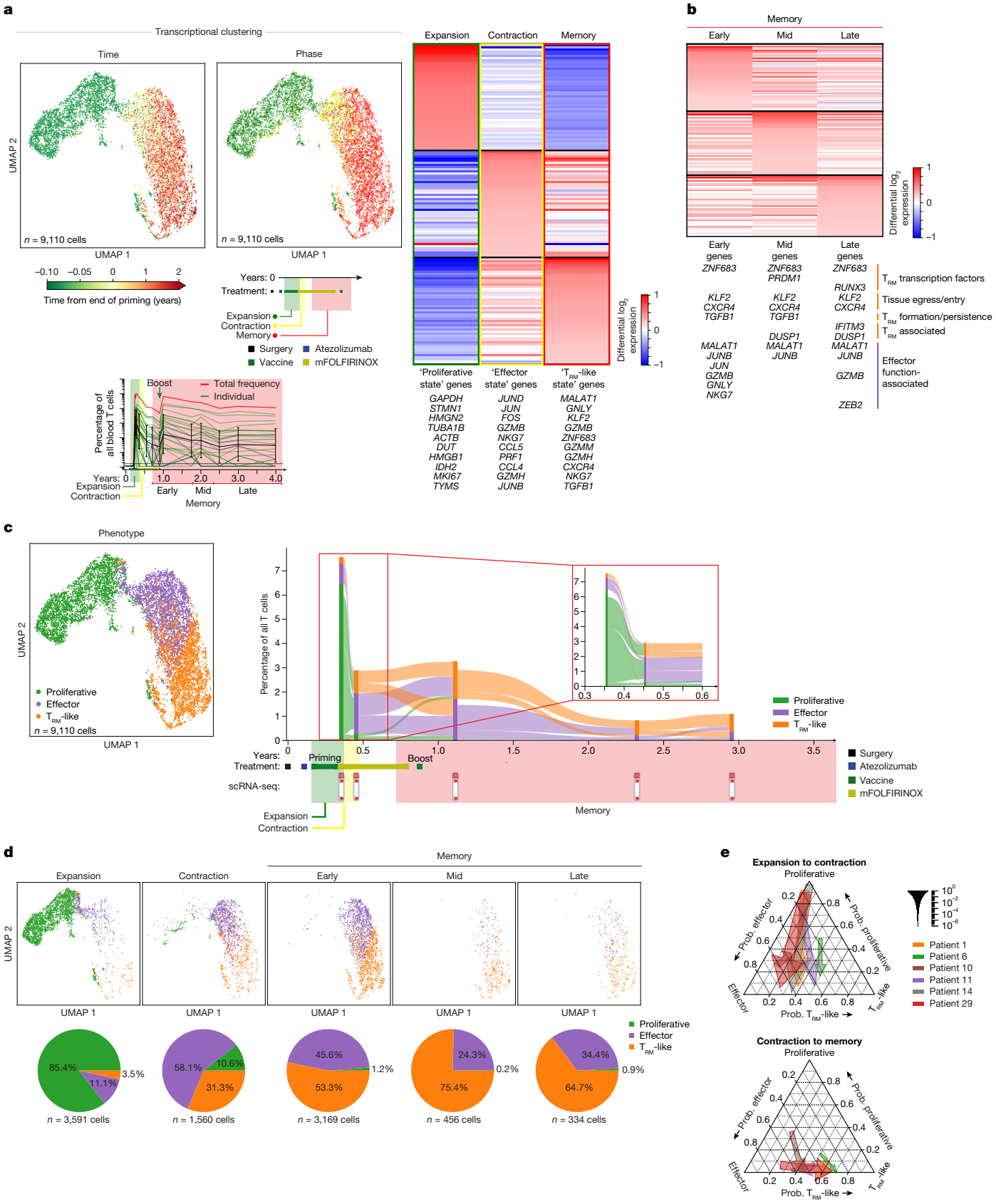

Fig. 3 | See next page for caption.

doses, we longitudinally traced contraction rates of clones in peripheral blood over time. With deep longitudinal sampling of clones (Fig. 2a), we can accurately fit a standard exponential function to the observed clonal decay dynamics (Extended Data Fig. 4e, top), and thus estimate the half-life and lifespan (time from peak frequency to below detection threshold; Methods) of each clone.

Fig. 3 | mRNA vaccine-induced clones converge in memory phase to effector T cells. a–**e**, Longitudinal phenotypes of 68 out of 71 CloneTrack clones in blood from 6 vaccine responders by single-cell RNA and TCR sequencing. **a**, Top left, uniform manifold approximation and projection (UMAP) plots of CloneTrack clone T cells by post-vaccination time and phase. Bottom left, schematic of CloneTrack clone phases in patient 1. **a**,**b**, Top 50 differentially expressed genes in CloneTrack clone T cells by phase relative to other phases (**a**, right) and by memory subphase relative to other subphases (**b**). Gene lists include genes that are characteristic of proliferative, effector and T_{RM} cells overexpressed by phase or subphase (a full gene list is provided in Supplementary Table 1). **c**, Left, transcriptional clustering of CloneTrack clone T cells by phenotype from single-cell RNA-sequencing (scRNA-seq) data. Right, PhenoTrack plot of phenotype composition and conversion of 68 out of 71 CloneTrack clones over time in 6 responders. Vertical coloured bars show the proportion of cells of each phenotype at corresponding times. Individual PhenoTrack plots are shown in Extended Data Fig. 8b. **d**, UMAP (top) and phenotype composition (bottom) of CloneTrack clone T cells post-vaccination. **e**, Phenotype conversion of CloneTrack clones from expansion to contraction (top) and contraction to memory (bottom) in $n = 6$ primed and boosted responders with persistent clones. Phenotype is plotted as probability (prob.) of each phenotype for clones from each responder. Patient 25 had no persistent clones and was analysed individually in Fig. 5a. Patient 5 did not receive a boost. Arrow width indicates clone frequency aggregated across patients; proximity of arrow base to the axis indicates fraction of cells per patient in a phenotype; arrows point from phenotype origin to destination. *n* is the number of cells or clones.

After vaccine priming, CloneTrack clones had an estimated median lifespan of 1.1 years (range 0.3 to approximately 100 years; Fig. 2c, top left), with a median half-life of approximately 40 days (Extended Data Fig. 4d, bottom). Notably, a single vaccine boost markedly extended estimated clone lifespan sevenfold to a median lifespan of 7.7 years, with lifespans ranging from 1.5 to 100 years (or possibly more than approximately 100 years; Methods) (Fig. 2c, top left; median half-life 297 days; Extended Data Fig. 4d). Thus, post-boost, in 5 of 7 patients, median estimated clone lifespans exceeded the 3-year post-surgery window where the majority (approximately 80%) of patients with PDAC historically recur[2–4] (Fig. 2c, bottom). Remarkably, in 4 out of 7 boosted patients, several clones (accounting for 30% ($n = 20$ out of 65) of all observed clones post-boost) had estimated lifespans that surpassed a decade (Fig. 2d, left). Peak expansion frequency correlated with clone lifespan (as expected from exponential decay) but not with half-life (Extended Data Fig. 4f). Additionally, CloneTrack clones that expanded with only one other clone had approximately sevenfold longer lifespan (post-prime) compared with clones that co-expanded with multiple clones (Extended Data Fig. 4g), which suggests that clone lifespan may increase with fewer competing clones. Clone lifespans were marginally longer in patients with polytopic (multiple immunogenic vaccine neoantigens) compared with monotopic (single immunogenic vaccine neoantigen) responses post-prime, but were similar post-boost (Extended Data Fig. 4h). Finally, CloneTrack clone lifespans reflect bona fide features of neoantigen-specific clones, as CloneTrack clones experimentally validated as specific for a neoantigen included in the vaccine (neoantigen-specific; Extended Data Fig. 3a,b) exhibited comparable half-lives and lifespans to other CloneTrack clones (Extended Data Fig. 4i).

To corroborate estimated clone lifespans with observed lifespans, we next examined whether CloneTrack clones persisted in the peripheral blood over time. Consistent with accurate exponential fits over the observed time frame (Extended Data Fig. 4e, bottom), estimated clone lifespan in responders closely correlated with observed lifespan (Fig. 2c, top right). Additionally, in the 7 evaluable patients with immunologic follow-up extending beyond 2 years post-vaccination (median immunologic follow-up 2.95 years post-vaccination), 86% (median) of CloneTrack clones (Fig. 2d, right) persisted to occupy substantial fractions of all blood T cells (median 0.07%), including as high as 1.1% approximately 3.8 years post-vaccination (Fig. 2e). In boosted patients, of CloneTrack clones that persisted 2 years post-vaccination (persistent clones; $n = 6$ patients), 87% were present at the time of boost, whereas 64% of non-persistent clones had disappeared from circulation before boost administration (Fig. 2f). Persistent clones trended to higher generation probabilities[5] (P_{gen}; Extended Data Fig. 5a), an estimate of preferential skewing of the human repertoire to generate specific TCRs through VDJ recombination, suggesting that compared with non-persistent clones, persistent clones may contain TCRs with higher likelihood of generation. Notably, vaccines did not co-expand clones that shared TCR Vβ specificity groups[6] with CloneTrack clones (Extended Data Fig. 5b,c). In sum, autogene cevumeran induces multiple $CD8^+$ T cell clones that persist long term in patients with PDAC, with latent lifespans that exceed the PDAC recurrence window and select clones that may outlive the host.

Long-lived clones are primed de novo

To probe the origin of long-lived CloneTrack clones, we used TCR Vβ sequencing to comprehensively search for CloneTrack clones in pre-vaccination host blood and tissues (tumours, tumour-draining lymph nodes (DLNs) and tumour-adjacent non-lymphoid tissues; 736,000 clones, 36 samples) in the 8 responders (Fig. 2a).

We detected only 2 cells of 2 CloneTrack clones pre-existing in host tissues: 1 cell in 319,000 tumour T cells and 1 cell in 233,000 T cells from tumour-adjacent tissue (Fig. 2g, top). No vaccine-induced cells resided among 18,100 DLN or 817,000 blood T cells (Fig. 2g, top). Out of the 79 CloneTrack clones, we detected only 2.5% pre-treatment (Fig. 2g, bottom left) among a total pool of 736,000 clones (1.4 million T cells; Fig. 2a). By contrast, 73% of anti-PD-L1-expanded clones (16 out of 22 clones expanded in vaccine responders by CloneTrack**;** Extended Data Fig. 6a) existed pre-treatment in single or multiple host compartments, with variable clone sizes (Fig. 2g, bottom right and Fig. 2h). Similar to the CloneTrack clones, only 6 out of the 58 neoantigen-specific clones identified in vitro (neoantigen-specific plus neoantigen-mapped clones; Extended Data Fig. 3a–c) in 8 responders pre-existed in any host tissues (Extended Data Fig. 3d). Thus, in patients with PDAC, unlike anti-PD-L1, which amplifies pre-existing clones, autogene cevumeran primes multiple naive clones that are undetectable in pre-vaccination host tissues to high magnitudes de novo.

Clones converge to effector T cells

As autogene cevumeran induced multiple T cell clones to persist long term in blood, to capture complete phenotypic histories of CloneTrack clones over time, we developed a computational strategy (PhenoTrack) that utilizes single-cell RNA and TCR sequencing to track the phenotypes of 9,110 single T cells of nearly all (68 out of 71) CloneTrack clones in the 6 responders who received both vaccine prime and boost doses and in whom clones persisted to approximately 3 years post-vaccination.

First, we noted that across patients, CloneTrack clones were, as previously described[1], primarily $CD8^+$ T cells (Extended Data Fig. 7a), with transcriptional signatures that segregated according to post-vaccination times when clones expanded (expansion phase, during vaccine priming), contracted (contraction phase, the end of vaccine priming to initiation of mFOLFIRINOX), and would be expected to persist as memory T cells[7] (memory phase, post-contraction; Fig. 3a, left). CloneTrack clones in the expansion phase overexpressed genes characteristic of proliferating cells (*MKI67* and others by Gene Set Enrichment Analysis (Methods); proliferative state) relative to all other phases, whereas effector genes (*GZMB*, *GZMH*, *NKG7*, *PRF1* and JUN family genes; effector state) were modulated in the contraction phase

(Fig. 3a, right and Supplementary Table 1). By contrast, CloneTrack clones that persisted in the memory phase did not differentially overexpress conventional markers of central or effector memory T cells[8] (including *SELL*, *TCF1*, *IL7R*, *CCR7* and others; Extended Data Fig. 7b) but instead overexpressed effector genes (*GZMB*, *GZMM*, *GZMH*, *GNLY*, *NKG7* and JUN family genes) and the core transcription factor of $CD8^+$ tissue-resident memory T (T_{RM}) cells (*ZNF683* (also known as *HOBIT*); T_{RM}-like state; Fig. 3a, right and Supplementary Table 1)[9]—long-lived T cells that reside in tissues and exhibit potent effector function upon antigen rechallenge[9], but may also circulate[10] and restrain cancer cells in dormancy in low antigen burden states[11]. These findings suggest that autogene cevumeran-primed T cells proliferate early, then contract, retain effector features and persist long term in a possible T_{RM}-like state that is endowed with circulatory capability.

As the memory phase spanned 2.5 years post-vaccination, we next subdivided the memory phase into early (0.8–1.8 years), mid (1.9–2.3 years) and late (beyond 2.4 years) memory phases (Fig. 3b and Supplementary Table 1) to further probe whether CloneTrack clones acquired T_{RM}-like features over time. Aligned with a T_{RM}-like phenotype with circulatory capability, relative to all other phases, CloneTrack clones not only overexpressed the core T_{RM} transcription factor gene *ZNF683*[12] selectively throughout all memory phases, but also progressively co-overexpressed the other two hallmark T_{RM} transcription factor genes *PRDM1*[12] (also known as *BLIMP1*) and *RUNX3*[13] in later memory phases (Fig. 3b). Furthermore, CloneTrack clones in the memory phase also overexpressed the transcription factor gene *KLF2*, which promotes tissue egress[8,14], *CXCR4*, which promotes tissue entry, *TGFB1*, which may promote T_{RM} formation and persistence[8,15] and T cell stemness[8] (Fig. 3b), poorly expressed tissue retention receptors (Extended Data Fig. 7c) and progressively retained and overexpressed effector (*GZMB*, JUN family, *ZEB2* and *MALAT1*)[16–18] and other T_{RM}-associated (*IFITM3* and *DUSP1*)[19,20] genes (Fig. 3a,b). CloneTrack clones in the memory phase did not express phenotypic markers on the T cell exhaustion continuum[8,21] (Extended Data Fig. 7d). Collectively, these data strongly suggest that autogene cevumeran induces $CD8^+$ T cells that persist long term in the circulation and do so in a stable non-exhausted T_{RM}-like effector state.

Next, as CloneTrack clones exhibited three distinct post-vaccination states (proliferative state during expansion, effector state during contraction and T_{RM}-like state during memory phase; Fig. 3a), we sought to examine how individual clone phenotypes transitioned over time. We assigned single cells to phenotypes associated with proliferative, effector and T_{RM}-like states (Fig. 3c, left, Extended Data Fig. 8a and Methods) and visualized clone phenotypic transitions using Sankey plots (Fig. 3c, right and Extended Data Fig. 8b), which differ from standard Sankey and alluvial plots by tracking phenotypes for clones as they expand and contract.

In the expansion phase, 85% of CloneTrack clone cells assumed the proliferative state, 11% assumed the effector state and 3.5% were in the T_{RM}-like state (Fig. 3d). Clones then rapidly contracted over 5 weeks and transitioned (Fig. 3c, right inset) from the proliferative state to primarily the effector (58% of vaccine-induced T cells) and the T_{RM}-like (31% of vaccine-induced T cells) states in the contraction phase (Fig. 3d), with cells of individual $CD8^+$ T cell clones assuming all phenotypes (Fig. 3e, top and Extended Data Fig. 8c, top). Entering the memory phase, clones remained in both cell states—although they were predominantly T_{RM}-like—over the next 2.5 years, thus retaining effector features despite the patients receiving mFOLFIRINOX after prime and subsequent boost doses (Fig. 3c,d). As in the proliferative to contraction transition, single clones simultaneously persisted in both cell states from contraction into memory (Fig. 3e, bottom and Extended Data Fig. 8c, bottom). In sum, autogene cevumeran induces $CD8^+$ T cell clones de novo that converge long term to T_{RM}-like and effector T cells, which are potentially poised to respond to antigen rechallenge.

To test whether the persistence of CloneTrack clones in responder blood correlated with preserved neoantigen-specific functional recall long term, we serially rechallenged peripheral blood mononuclear cells (PBMCs) isolated post-priming to approximately 3.6 years post-vaccination (approximately 3.8 years post-surgery) with ELISpot-positive vaccine neoantigens in vitro and examined $CD8^+$ T cell cytokine production and lytic capacity (Fig. 4a). Overall, $CD8^+$ T cells in all vaccine responders produced cytokines (IFNγ and TNFα) and degranulated on neoantigen rechallenge post-priming (Fig. 4a) and continued to produce effector cytokines and display lytic potential up to 3.6 years post-vaccination in 6 of 8 vaccine responders (Fig. 4a,b). Specifically, in 4 out of 4 monotope responders (Extended Data Fig. 9a) and 2 out of 4 polytope responders (Fig. 4a, bottom, c and Extended Data Fig. 9b), $CD8^+$ T cells continued to produce IFNγ and TNFα and degranulated upon in vitro neoantigen rechallenge with previously determined[1] ELISpot-positive dominant and subdominant vaccine neoantigens up to 3.6 years post-vaccination. Moreover, loss of neoantigen functional recall roughly correlated with clonal persistence, as both patients without recall exhibited polytopic responses with the lowest aggregate CloneTrack clone frequencies in the blood at late post-vaccination times (patients 10 and 25; Fig. 4c, right), suggesting that CloneTrack clones that persist can mediate effector function. To further characterize features of long-lived vaccine-induced clones, we mapped the avidity of 12 TCRs, including 10 CloneTrack clones and 2 vaccine neoantigen-specific clones identified in vitro (Extended Data Fig. 3b) that persisted long term (median lifespan 8.8 years) in 3 responders (Fig. 4d). TCRs of vaccine-induced clones displayed lower half-maximal effective concentration (EC_{50}) and higher avidity to cognate neoepitopes compared with wild-type epitopes and included neoepitope–TCR pairs with nano- and subnanomolar avidity (Fig. 4d, bottom right), confirming that passenger mutations in PDAC—a tumour with low mutational burden—can generate high-avidity neoepitopes that are recognized by endogenous T cells. Furthermore, higher relative avidity of TCRs to the neoepitope compared with the wild-type epitope (higher log (C)) correlated with shorter clone half-life after prime but not after boost (Fig. 4d), suggesting that higher relative epitope strength may correlate with rate of clonal decay. Together, these results indicate that in patients with PDAC, autogene cevumeran induces $CD8^+$ T cell clones, including clones with high avidity to PDAC neoepitopes, that persist up to 3.6 years post-vaccination, retain multiple effector function long term, and display the potential to persist for decades.

Vaccine immunity and cancer relapse

As two responders (patients 25 and 14) recurred during the observation period, we explored whether variations in vaccine immunity correlated with PDAC recurrence. Patient 25—a polytope responder, the first responder to recur, and the only responder to die (from locally recurrent PDAC)—had an approximately tenfold shorter observed T cell lifespan compared with other responders (Fig. 5a, left). All six CloneTrack clones steeply declined after the eight priming doses (Extended Data Fig. 2a). Notably, in this patient, the boost dose re-expanded but did not rescue primed CloneTrack clones, with subsequent disappearance of CloneTrack clones prior to death of the patient (Extended Data Fig. 2a). This shorter T cell longevity was not owing to distinct post-priming phenotypes (Fig. 5a, bottom). Similar to other responders (Fig. 3c,e and Extended Data Fig. 8b,c), CloneTrack clones from this patient were a mix of proliferative and effector phenotypes post-priming that converged to the T_{RM}-like state. Patient 14—a monotope responder, and the second responder to recur (stable, solitary 1-cm lung metastasis)—had an altered treatment sequence, resulting in later onset of CloneTrack clones (34 weeks post-surgery) compared with the other 7 responders (median 13 weeks after surgery; Fig. 5a, middle), with clones similarly adopting effector and T_{RM}-like states in the memory phase (Extended Data Fig. 8b). Thus, both individuals who recurred had weaker cumulative vaccine immunity (aggregate CloneTrack clone T cells integrated over the follow-up window; Fig. 5a, right) due to shortest longevity or latest onset.

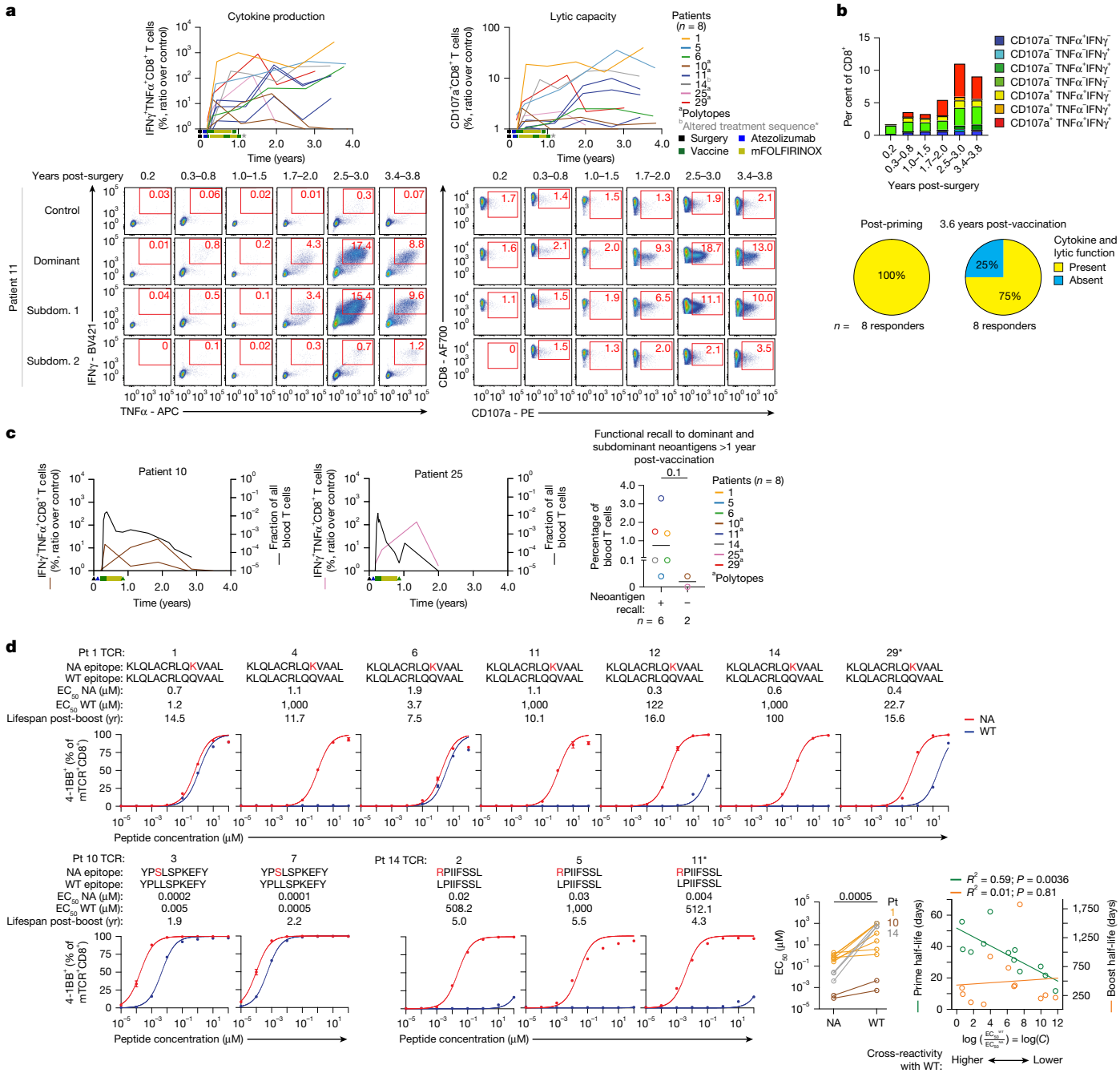

Fig. 4 | Vaccine-induced T cells retain multiple effector functions long term. a–**c**, Longitudinal cytokine production and lytic capacity of CD8$^+$ T cells after in vitro rechallenge with immunodominant and subdominant (subdom.) ELISpot-positive vaccine neoantigens in responders. **a**, Top, post-rechallenge aggregate percentage of IFNγ$^+$TNFα$^+$CD8$^+$ T cells (cytokine production) and CD107a$^+$CD8$^+$ T cells (lytic capacity) in responders. The *y* axis shows the ratio of neopeptide-activated T cell fraction to the DMSO-activated T cell fraction. Asterisk (*) indicates altered treatment sequence for patient 14. Bottom, representative flow cytometry of T cells from a vaccine responder. **b**, Longitudinal median percentage of CD8$^+$ T cell subsets (top) and percentage of responders with polyfunctional (cytokine$^+$CD107a$^+$) vaccine neoantigen-specific CD8$^+$ T cells (bottom) after in vitro neoantigen rechallenge. **c**, Left, aggregate fraction of CloneTrack clone T cells in blood and percentage of IFNγ$^+$TNFα$^+$CD8$^+$ T cells after in vitro rechallenge in two responders with waning immunity. Right, aggregate percentage of CloneTrack clone T cells in blood stratified by responders with or without neoantigen-specific IFNγ$^+$TNFα$^+$CD8$^+$ T cells more than one year post-vaccination by in vitro rechallenge. **a**–**c**, Dominant and subdominant neoantigens are vaccine neoantigens that were previously determined[1] to elicit IFNγ$^+$ T cells by ex vivo IFNγ ELISpot in PBMCs collected 1–3 weeks post vaccine priming (dominant neoantigens elicit a maximal T cell response; subdominant antigens elicit a non-maximal T cell response). DMSO was used as a control. **d**, Avidity (left) and EC_{50} values (right) for TCR-transduced CD8$^+$ T cells cultured with human leukocyte antigen (HLA)-matched, neopeptide or wild-type (WT) peptide-pulsed antigen-presenting cells. TCRs isolated from CloneTrack or neoantigen-specific clones (asterisk) are identified as in Extended Data Fig. 3a–c. Residues shown in red are mutated amino acids. log(*C*) is the antigenic distance[28]. Flow cytometry is gated on live CD3$^+$CD56$^-$CD8$^+$ cells (**a**) or live CD3$^+$CD8$^+$ TCR-transduced cells (**d**). *n* is the number of patients. *P* values by two-tailed Mann–Whitney test (**c**, right) and two-sided Wilcoxon matched-pairs signed rank test (**d**, bottom right). Error bars in **d** indicate s.e.m.

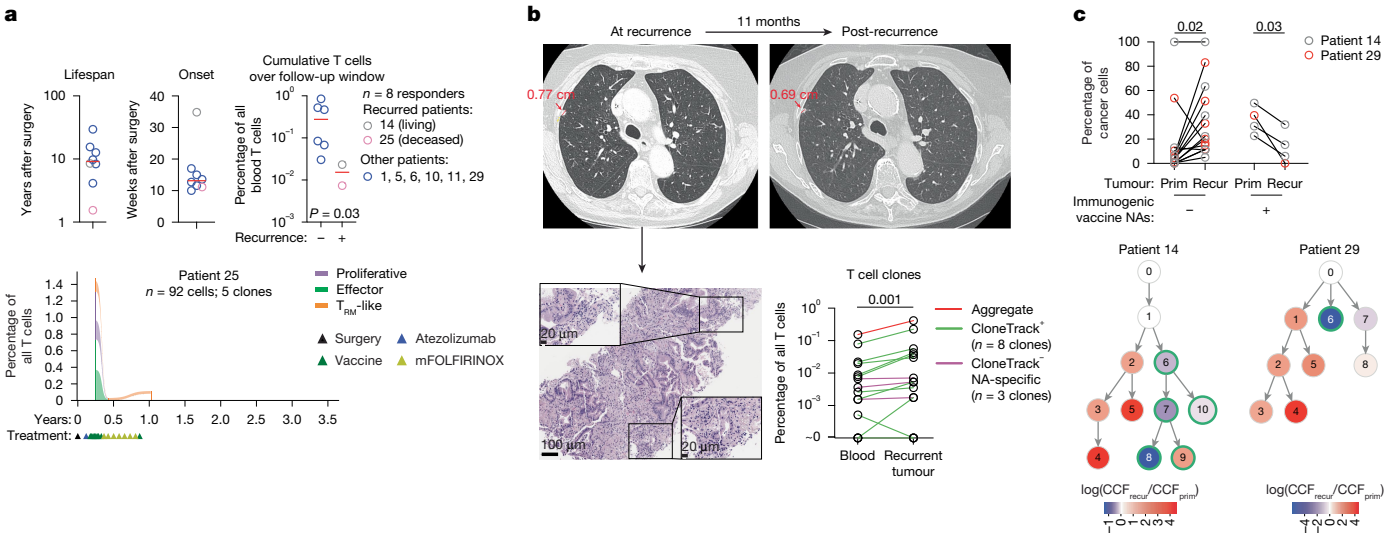

Fig. 5 | Vaccine immunity and neoantigen editing in patients with recurrent PDAC. a, Top, estimated lifespan (left), observed time of onset (middle) and cumulative frequency (right) of vaccine-induced CloneTrack clone T cells over the observation period in responders with or without recurrence. Bottom, longitudinal phenotype of CloneTrack clone T cells in patient 25. **b**, Computed tomography (top; with tumour diameter in red) and histopathology (bottom left) of the solitary lung metastasis from patient 14. Bottom right, vaccine-induced T cell clones in blood and a recurrent tumour from patient 14. CloneTrack$^+$, blood T cell clones identified by CloneTrack as in Extended Data Fig. 2a; CloneTrack$^-$ NA-specific, blood T cell clones identified as neoantigen-specific in vitro as in Extended Data Fig. 3a–c. **c**, Percentage (top) and phylogeny (bottom) of cancer clones in primary and recurrent tumours that harbour immunogenic and non-immunogenic vaccine neoantigens (as determined by ex vivo IFNγ ELISpot[1]) in patients 14 and 29. Prim, primary tumour; Recur, recurrent tumour. Red and blue indicate increasing and decreasing cancer clone fraction (CCF) from primary to recurrent tumours, respectively. Green circles indicate clones with immunogenic vaccine neoantigens. *n* is the number of patients, cells or clones. *P* values by two-tailed Mann–Whitney test (**a**, right), two-tailed Wilcoxon matched-pairs signed rank test (**b**, bottom) and two-tailed paired *t*-test (**c**, top).

To examine whether CloneTrack clones retained function to infiltrate recurrent tumours, we searched for CloneTrack clones in the solitary lung metastasis of patient 14 (Fig. 5b, top). Seven out of the eight CloneTrack clones that persisted in the late memory phase were clonally expanded in the recurrent tumour compared with blood (Fig. 5b, bottom). Additionally, three neoantigen-specific clones identified in vitro but not by CloneTrack (Extended Data Fig. 3b) were also present in the recurrent tumour (Fig. 5b), suggesting that both CloneTrack and in vitro-identified neoantigen-specific clones retained in vivo function to infiltrate distant tumours. To further examine whether these T cell clones were exerting selective pressure on clinically undetectable tumour clones, we tested whether vaccine-induced immunity could exert selective pressure on tumour clones carrying immunogenic vaccine neoantigens, either directly through selective loss of vaccine-targeted tumour clones, or indirectly through acquired immunity against neoantigens that were not included in the vaccine. We did not detect clear evidence of acquired immune activity (which would suggest neoepitope spread) against tumour mutational neoantigens that were not included in vaccines in any responder (Extended Data Fig. 10). However, using whole-exome sequencing and phylogenetic analyses, we examined how primary PDACs longitudinally evolved to recurrence in patient 14 and patient 29—a patient who was previously reported[1] to develop a disappearing solitary liver micrometastasis (criteria for clinical recurrence not met) infiltrated by vaccine-induced T cell clones. Consistent with vaccine-induced immunity exerting selective pressure on micrometastatic tumour clones, recurrent tumours from both patients evolved with fewer tumour clones carrying immunogenic vaccine neoantigens (Fig. 5c).

Discussion

Can we overcome host tolerance to generate strong, specific, functional and durable T cells against a tumour antigen? If so, which antigens, vaccines and hosts can collectively generate such a response? Here in PDAC, one of the most lethal and oncologically challenging cancers, which kills 88% of patients[22], we show that autogene cevumeran, an unmodified uridine-based mRNA–lipoplex vaccine that targets somatic mutation-derived neoantigens, administered in patients with minimal disease burden, may offer a composite solution to this challenge.

The substantial longevity and functionality of vaccine-induced CD8$^+$ T cell clones identified by CloneTrack following fixed prime-boost vaccination is notable. Vaccine-induced CloneTrack clones exhibit estimated multiyear lifespans, with nearly a quarter of clones estimated to have multi-decade lifespans, longer than conservatively estimated patient lifespans. Notably, these cells exhibit robust neoantigen-specific T cell polyfunctionality for up to 3.6 years post-vaccination. Furthermore, vaccine-induced clones can infiltrate recurrent PDACs, as observed previously in one patient[1] and in a second in this study. Although one patient (patient 1) contributed a large number of clones to the pool of vaccine-induced clones, subset analysis in individual patients reveals substantial estimated longevity of clones in all individual boosted patients. These lifespan estimates will require additional experimental validation in future work. Nevertheless, they indicate that it is possible to generate long-lived, functional CD8$^+$ T cells that are specific for a tumour antigen without repetitive boosting in diseased hosts. Our vaccination strategy and the mRNA vaccine platform appear to surpass several vaccine litmus tests—the magnitude of vaccine-induced CD8$^+$ T cells that persist over time in steady state appears comparable, if not higher, than that of vaccine-induced CD8$^+$ T cells observed with highly successful pathogen vaccines[23], where even single immunizations confer lifetime immunity[24]. Furthermore, vaccine-induced long-term immunity consists predominantly of CD8$^+$ T cells, mimicking possible 'natural' immunologic control in PDAC[25]. However, we cannot rule out that vaccines also induce CD4$^+$ T cells. Crucially, vaccine-induced immunity spans the PDAC recurrence window, thus potentially conferring protection throughout the period of highest susceptibility, a desired feature for a cancer vaccine. Although we demonstrate that unmodified mRNA lipoplexes that target neoantigens

in minimally diseased hosts trigger lasting immunity, it remains to be seen whether vaccines that target other antigen classes or utilize emerging vaccine platforms can achieve similar durable functionality.

We cannot exclude that vaccine-induced T cell clones may be present in tumour or lymph node regions that were not sampled in this study. However, it is notable that despite the relatively low mutational burden of PDAC and thus its presumed lower neoantigen content, autogene cevumeran, a uridine-based mRNA neoantigen vaccine, primes long-lived T cells de novo against passenger mutations rather than amplifying pre-existing CD8$^+$ T cells. Given that such neoantigens are fundamental byproducts of oncogenesis, and adjuvant therapy in minimally diseased hosts is a ubiquitous cancer treatment paradigm, our findings expand the theoretical vaccine-eligible pool to nearly all cancers, and not only those that elicit a robust endogenous neoantigen-specific T cell response. Immunologically cold tumours with few mutations, such as gastrointestinal cancers, appear to be ideal initial disease indications, given the often relatively low mutational burden, insensitivity to immune checkpoint inhibitors, continued reliance on last-generation cytotoxic chemotherapy as standard treatment and poor prognosis.

Although we find that lower cumulative vaccine immunity correlates with early recurrence in responders, the significance of this observation is limited by the small sample size. Nevertheless, the observation further supports the hypothesis that adjuvant autogene cevumeran may delay PDAC recurrence. Indeed, we report durable correlations between vaccine response and RFS at 3.2-year follow-up with a similar effect size to that observed at an earlier 1.5-year follow-up[1]. Although we did not previously detect[1] (and currently selectively confirm) differences in responder and non-responder treatment, tumour or host immune fitness, unknown factors may confound the correlation between vaccine response and RFS. Nevertheless, utilizing complete clonal histories of more than 9,000 single cells in 6 patients, we show that most vaccine-induced CD8$^+$ T cell clones transition into the memory phase as stable effector T cells, and provide comprehensive characterization of the longitudinal state transitions and long-term phenotypes of mRNA cancer vaccine-induced T cells. Notably, the vaccine-induced T cells that persist into the memory phase do not acquire exhaustion features despite multiple priming doses[26], and may phenotypically resemble human T_{RM} cells with circulatory function described in mice[10]. Of note, loss of vaccine-induced neoantigen-specific functionality is not associated with longitudinal T cell phenotypic change but appears linked to loss of the neoantigen-specific T cells themselves. Although it remains unknown whether vaccine-induced T cells retain this effector function within tumours, this observation opens the possibility to maintain or rescue immunity with real-time monitoring and scheduled or on-demand boosting. Although speculative, a vaccine T cell 'titre' to dynamically monitor and boost T cells—as we show is feasible with CloneTrack—can empower such advances and warrants future investigation.

That the mutational profile of recurrent PDACs evolved under vaccine-induced selective pressure is both predictable and notable. Although we did not observe this clonal pruning together with T cell immunity spreading to non-vaccinated mutational neoantigens, this finding suggests that vaccine-induced T cells target subclinical cancer clones, and consequently, one mechanism of vaccine resistance may be clonal escape. Notably, a lack of observed neoantigen spread does not rule out immunity spreading to other mutational or non-mutational antigens, as the neoantigens tested in our study may be non-immunogenic. Indeed, neoantigen spread may be more prominently observed in settings of higher neoantigen burden[27], such as in more highly mutated cancers that elicit stronger endogenous immunity and may not be an observed feature in a tumour with fewer mutations. Nonetheless, effective cancer vaccines may require initial polyvalent vaccines that target all heterogeneous cancer clones, with subsequent neoantigen resampling and adaptive vaccination to target clonal escapes or, alternatively, vaccines that induce T cells against clonal neoantigens with high potency and durability.

In sum, we present additional evidence with longer follow-up that autogene cevumeran—a uridine-based mRNA vaccine against somatic mutation-derived neoantigens—can generate strong, specific, functional and durable CD8$^+$ T cell immunity in PDAC that correlates with delayed recurrence. A global randomized trial (IMCODE 003; NCT05968326) is ongoing. As mutation-derived neoantigens are fundamental features of transformed cells, our findings provide support for broad testing of mRNA neoantigen vaccines as adjuvant cancer therapies.

Online content

Any methods, additional references, Nature Portfolio reporting summaries, source data, extended data, supplementary information, acknowledgements, peer review information; details of author contributions and competing interests; and statements of data and code availability are available at https://doi.org/10.1038/s41586-024-08508-4.

1. Rojas, L. A. et al. Personalized RNA neoantigen vaccines stimulate T cells in pancreatic cancer. *Nature* **618**, 144–150 (2023).
2. Neoptolemos, J. P. et al. Adjuvant chemotherapy with fluorouracil plus folinic acid vs gemcitabine following pancreatic cancer resection: a randomized controlled trial. *JAMA* **304**, 1073–1081 (2010).
3. Uesaka, K. et al. Adjuvant chemotherapy of S-1 versus gemcitabine for resected pancreatic cancer: a phase 3, open-label, randomised, non-inferiority trial (JASPAC 01). *Lancet* **388**, 248–257 (2016).
4. Neoptolemos, J. P. et al. Comparison of adjuvant gemcitabine and capecitabine with gemcitabine monotherapy in patients with resected pancreatic cancer (ESPAC-4): a multicentre, open-label, randomised, phase 3 trial. *Lancet* **389**, 1011–1024 (2017).
5. Murugan, A., Mora, T., Walczak, A. M. & Callan, C. G. Statistical inference of the generation probability of T-cell receptors from sequence repertoires. *Proc. Natl Acad. Sci. USA* **109**, 16161–16166 (2012).
6. Glanville, J. et al. Identifying specificity groups in the T cell receptor repertoire. *Nature* **286**, 958 (2017).
7. Sallusto, F., Lanzavecchia, A., Araki, K. & Ahmed, R. From vaccines to memory and back. *Immunity* **33**, 451–463 (2010).
8. Gebhardt, T., Park, S. L. & Parish, I. A. Stem-like exhausted and memory CD8$^+$ T cells in cancer. *Nat. Rev. Cancer* **23**, 780–798 (2023).
9. Buggert, M., Price, D. A., Mackay, L. K. & Betts, M. R. Human circulating and tissue-resident memory CD8$^+$ T cells. *Nat. Immunol.* **24**, 1076–1086 (2023).
10. Fonseca, R. et al. Developmental plasticity allows outside-in immune responses by resident memory T cells. *Nat. Immunol.* **21**, 412–421 (2020).
11. Park, S. L. et al. Tissue-resident memory CD8$^+$ T cells promote melanoma–immune equilibrium in skin. *Nature* **565**, 366–371 (2019).
12. Mackay, L. K. et al. Hobit and Blimp1 instruct a universal transcriptional program of tissue residency in lymphocytes. *Science* **352**, 459–463 (2016).
13. Milner, J. J. et al. Runx3 programs CD8$^+$ T cell residency in non-lymphoid tissues and tumours. *Nature* **552**, 253–257 (2017).
14. Carlson, C. M. et al. Kruppel-like factor 2 regulates thymocyte and T-cell migration. *Nature* **442**, 299–302 (2006).
15. Crowl, J. T. et al. Tissue-resident memory CD8$^+$ T cells possess unique transcriptional, epigenetic and functional adaptations to different tissue environments. *Nat. Immunol.* **23**, 1121–1131 (2022).
16. Kragten, N. A. M. et al. Blimp-1 induces and Hobit maintains the cytotoxic mediator granzyme B in CD8 T cells. *Eur. J. Immunol.* **48**, 1644–1662 (2018).
17. Chen, J. et al. NR4A transcription factors limit CAR T cell function in solid tumours. *Nature* **567**, 530–534 (2019).
18. Wheeler, B. D. et al. The lncRNA Malat1 inhibits miR-15/16 to enhance cytotoxic T cell activation and memory cell formation. *eLife* **12**, RP87900 (2023).
19. Wakim, L. M., Gupta, N., Mintern, J. D. & Villadangos, J. A. Enhanced survival of lung tissue-resident memory CD8$^+$ T cells during infection with influenza virus due to selective expression of IFITM3. *Nat. Immunol.* **14**, 238–245 (2013).
20. Ostkamp, P. et al. A single-cell analysis framework allows for characterization of CSF leukocytes and their tissue of origin in multiple sclerosis. *Sci. Transl. Med.* **14**, eadc9778 (2022).
21. Giles, J. R., Globig, A.-M., Kaech, S. M. & Wherry, E. J. CD8$^+$ T cells in the cancer-immunity cycle. *Immunity* **56**, 2231–2253 (2023).
22. Siegel, R. L., Miller, K. D., Wagle, N. S. & Jemal, A. Cancer statistics, 2023. *Ca. Cancer J. Clin.* **73**, 17–48 (2023).
23. Akondy, R. S. et al. Origin and differentiation of human memory CD8 T cells after vaccination. *Nature* **552**, 362–367 (2017).
24. Marraco, S. A. F. et al. Long-lasting stem cell–like memory CD8$^+$ T cells with a naïve-like profile upon yellow fever vaccination. *Sci. Transl. Med.* **7**, 282ra48 (2015).
25. Balachandran, V. P. et al. Identification of unique neoantigen qualities in long-term survivors of pancreatic cancer. *Nature* **551**, 512–516 (2017).
26. Kranz, L. M. et al. Systemic RNA delivery to dendritic cells exploits antiviral defence for cancer immunotherapy. *Nature* **534**, 396–401 (2016).
27. Hu, Z. et al. Personal neoantigen vaccines induce persistent memory T cell responses and epitope spreading in patients with melanoma. *Nat. Med.* **27**, 515–525 (2021).
28. Łuksza, M. et al. Neoantigen quality predicts immunoediting in survivors of pancreatic cancer. *Nature* **606**, 389–395 (2022).

[1]Immuno-Oncology Service, Human Oncology and Pathogenesis Program, Memorial Sloan Kettering Cancer Center, New York, NY, USA. [2]Hepatopancreatobiliary Service, Department of Surgery, Memorial Sloan Kettering Cancer Center, New York, NY, USA. [3]The Olayan Center for Cancer Vaccines, Memorial Sloan Kettering Cancer Center, New York, NY, USA. [4]Computational Oncology Service, Department of Epidemiology and Biostatistics, Memorial Sloan Kettering Cancer Center, New York, NY, USA. [5]BioNTech, Mainz, Germany. [6]Genentech, San Francisco, CA, USA. [7]Meyer Cancer Center, Weill Cornell Medicine, Weill Cornell Medical College, New York, NY, USA. [8]Department of Pathology, Memorial Sloan Kettering Cancer Center, New York, NY, USA. [9]Department of Epidemiology and Biostatistics, Memorial Sloan Kettering Cancer Center, New York, NY, USA. [10]Department of Medicine, Memorial Sloan Kettering Cancer Center, New York, NY, USA. [11]David M. Rubenstein Center for Pancreatic Cancer Research, Memorial Sloan Kettering Cancer Center, New York, NY, USA. [12]HI-TRON, Helmholtz Institute for Translational Oncology, Mainz, Germany. [13]Physiology, Biophysics and Systems Biology, Weill Cornell Medicine, Weill Cornell Medical College, New York, NY, USA. [14]These authors contributed equally: Zachary Sethna, Pablo Guasp. [15]These authors jointly supervised this work: Benjamin D. Greenbaum, Vinod P. Balachandran. ✉e-mail: balachav@mskcc.org

Methods

Trial design, patients and endpoints

In our previously reported[1] single-centre, investigator-initiated, phase 1 clinical trial, patients with single, radiographically suspicious, surgically resectable PDAC, no distant metastases, and ≥5 neoantigens as predicted by our computational pipeline were treated with sequential surgery, adjuvant atezolizumab (anti-PD-L1), autogene cevumeran (an individualized vaccine based on uridine mRNA–lipoplex nanoparticles encoding up to 20 MHCI and MHCII restricted neoantigens) and mFOLFIRINOX. All patients had ECOG (Eastern Cooperative Oncology Group) performance status 0–1. We included patients with pathologically confirmed PDAC with surgical margin status R0/R1. We excluded patients with metastatic, borderline or locally unresectable PDAC and patients who received neoadjuvant therapy. The primary endpoint was safety. Secondary endpoints were 18-month RFS and 18-month OS. Additional eligibility criteria, procedures, treatments, and ethical study conduct have been described and are available in the protocol[1] (Supplementary File 1).

We treated 19 patients with atezolizumab (safety-evaluable cohort), of which 16 patients received subsequent autogene cevumeran (biomarker-evaluable cohort)[1]. Fifteen of these 16 patients received subsequent mFOLFIRINOX. As described previously[1], vaccinated patients were classified as autogene cevumeran (vaccine) responders if they generated high-magnitude T cell responses to vaccine neoantigens assessed by a previously described ex vivo IFNγ ELISpot assay[29] that detects vaccine-induced T cell responses and does not distinguish $CD8^+$ from $CD4^+$ T cell responses.

We defined recurrence as new lesions by response evaluation criteria in solid tumours (RECIST, version 1.1). We defined RFS from either the date of surgery (RFS) or from the date of the last autogene cevumeran priming dose (landmark RFS) to the date of recurrence or death, whichever occurred first. We defined OS from the date of surgery to the date of death. We censored patients without events at the last known date they were recurrence-free. We defined the recurrence window as the time frame from surgery when ~80% of patients recur[2–4]. Data cut-off was 1 December 2023, extending the median follow-up to 38 months.

We conducted the study in accordance with the Declaration of Helsinki and good clinical practice guidelines. The study was approved by the institutional review board (IRB) at Memorial Sloan Kettering Cancer Center (MSK), the United States Federal Drug Administration (FDA), and was registered on clinicaltrials.gov (NCT04161755). All participants provided written informed consent.

Mutation identification and neoantigen selection for personalized vaccines

We previously reported detailed characteristics of vaccine neoantigen selection[1]. In brief, we identified expressed non-synonymous mutations and HLA type by whole-exome sequencing of patient-specific tumour–normal pairs and tumour RNA sequencing. We then bioinformatically estimated neoantigens and ranked neoantigens by immunogenicity as previously described[30].

Autogene cevumeran manufacture

As reported[1], for every patient, we manufactured individualized mRNA neoantigen vaccines under good manufacturing practice conditions as two uridine-based mRNA strands with noncoding sequences optimized for superior translational performance[31,32]. We designed each strand to encode up to 10 MHCI and MHCII neoantigens formulated in approximately 400-nm diameter lipoplex nanoparticles[26] that comprised the synthetic cationic lipid (*R*)-*N*,*N*,*N*-trimethyl-2,3-diol eyloxy-1-propanaminiumchloride (DOTMA) and the phospholipid 1,2-dioleoyl-sn-glycero-3-phosphatidylethanolamine (DOPE) to enable intravenous delivery.

Patient samples, cell lines and cell culture

We purified patient PBMCs by density centrifugation over Ficoll-Paque Plus (GE Healthcare) and cultured purified cells in RPMI medium supplemented with 10% fetal bovine serum (FBS, Nucleus Biologics), 1 mM sodium pyruvate, 2 mM L-glutamine, non-essential amino acids and 2-mercaptoethanol, 100 U ml^{-1} penicillin-streptomycin (MSK medium preparation core facility), with 100 U ml^{-1} IL–2 (Peprotech) and 100 U ml^{-1} IL-15 (Peprotech) added every other day. To map single clone reactivity, we purchased pan negative selection purified human T cells (Precision for Medicine) and cultured purified T cells in RPMI medium (Gibco, Thermo Fischer Scientific) supplemented with 10% FBS (Sigma-Aldrich), 100 U ml^{-1} penicillin-streptomycin (Gibco, Thermo Fischer Scientific), 1,000 U ml^{-1} IL-7 (Peprotech, Thermo Fischer Scientific), 100 U ml^{-1} IL-15 (Peprotech, Thermo Fischer Scientific) and 4 mM L-glutamine (Gibco, Thermo Fischer Scientific). We cultured T2 and K562 cells with RPMI medium (Gibco, Thermo Fischer Scientific) supplemented with 10% FBS (Sigma-Aldrich) and 100 U ml^{-1} penicillin-streptomycin (Gibco, Thermo Fischer Scientific). We cultured Phoenix-AMPHO and RD114-envelope producer cells with DMEM medium (Gibco, Thermo Fischer Scientific) supplemented with 10% FBS (Sigma-Aldrich) and 100 U ml^{-1} penicillin-streptomycin (Gibco, Thermo Fischer Scientific). We froze tumour, adjacent tissue and draining lymphatic tissue samples from resected tumour specimens for subsequent analysis.

HLA cloning and transduction

We cloned patient-matched HLA alleles and transduced T2 and K562 cells as previously described[1]. In brief, we cloned HLA alleles followed by an IRES GFP reporter into a SFG γ-retroviral vector and transfected Phoenix-AMPHO cells using Lipofectamine 3000 (Thermo Fisher Scientific). We collected vector-containing supernatants and used them to transduce T2 and K562 cells by spinoculation in the presence of Polybrene (EMD Millipore). We sorted HLA^+ K562 cells and GFP^+ T2 cells using an Aria Cell sorter (BD Biosciences).

TCR reconstruction, cloning, transduction and peptide stimulation

We reconstructed and cloned TCRs as previously described[1]. In brief, we identified T receptor beta (TRB) V-D-J and T receptor alpha (TRA) V-J sequences from purified, sequenced single T cells and fused them to modified mouse constant TRB and TRA chain sequences, respectively. Then, we joined TRB and TRA chains with a furin SGSG P2A linker and cloned them into a SFG γ-retroviral vector. We transduced human pan T cells as previously described[1] with minor modifications. In brief, we transfected Phoenix-AMPHO cells with SFG γ-retroviral vectors using Lipofectamine 3000 (Thermo Fisher Scientific). Then, we used vector-containing supernatants to transduce RD114-envelope producer cells. We sorted transduced cells to generate stable cell lines and concentrated vector-containing supernatants using Retro-X Concentrator (Takara). We activated human pan T cells with CD3/CD28 beads (Thermo Fisher) and transduced them at day 3 post-activation in a Retronectin (Takara) coated plate using concentrated vector-containing supernatants. Transduction efficiency was confirmed by flow cytometry gating on live $CD8^+$ $mTCR^+$ cells.

To select possible neoantigen epitopes to test TCR specificity and binding, we generated all possible unique 8–14mers out of all full-length (18–27mer) immunogenic (ELISpot-positive) vaccine neoantigens. We predicted binding of each of these 8 to 14mers to the patient's HLA-I by NetMHCPan4.1. We further selected peptides with binding affinities <1000 nM or predicted strong binders (as per NetMHCPan4.1) for further testing and peptide stimulation.

We stimulated TCR-transduced T cells with peptides as follows: we pulsed 2.5×10^5 HLA-transduced T2 or K562 cells in a 96-well U-bottom plate at 37 °C with the indicated peptides at the indicated

concentrations for 1 h. Then, we centrifuged and washed the peptide, added 5×10^4 TCR (effector:target ratio of 1:5) or mock (control) transduced T cells per well, and measured CD137 (4-1BB) expression on $CD8^+$ mouse TCR^+ T cells after 24 h in coculture. To calculate the avidity of a TCR for its cognate epitope and the corresponding wild-type peptide, we stimulated TCR-transduced T cells with antigen-presenting cells pulsed with different concentrations of mutant or wild-type peptide (range from 100 μM to 10^{-5} μM), performed a nonlinear regression to fit the data to a sigmoidal curve, and calculated the EC_{50} as the peptide concentration that activates 50% of the TCR-transduced T cells. When a TCR did not show reactivity with an EC_{50} value tending towards infinite, we assigned the EC_{50} to be 1,000 μM.

Immune response

TCR Vβ sequencing. We extracted gDNA from bulk PBMCs, purified T cells and patient tissue samples using a DNA extraction kit (Qiagen). We used Dropsense 96 to quantify samples, dilute standard concentrations, and prepare libraries. We then generated sample data using an immunoSEQ Assay (Adaptive Biotechnologies), as previously described[1]. In brief, we amplified the somatically rearranged TCRB CDR3 using a two-step, amplification bias-controlled multiplex PCR reaction, that contains forward and reverse amplification primers specific to every known V and J gene segment and amplifies the CDR3 receptor hypervariable locus, followed by a second PCR to add barcode and Illumina adapter sequences[33]. Reference gene primers in the PCR further quantify total nucleated cells available for sequencing, and thus measure the fraction of T cells in each sequenced sample. The CDR3 and reference gene libraries were then sequenced, raw sequence reads demultiplexed per Adaptive's barcode sequences, and demultiplexed reads processed to remove adapter and primer sequences and identify and remove primer dimer, germline and contaminant sequences. Relative frequency ratios between similar clones and a modified nearest-neighbour algorithm were used to cluster the filtered results, and merge closely related sequences to correct for sequencing induced technical errors. The output sequences were then annotated to the V, D, and J genes and N1 and N2 regions that constitute each unique CDR3, and the corresponding encoded CDR3 amino acid sequence. We defined annotated genes per the IMGT database (https://www.imgt.org). The output TCR V CDR3 sequences were then normalized and corrected for residual multiplex PCR amplification bias and quantified versus synthetic TCRB CDR3 sequence analogues[34].

Single-cell RNA and TCR sequencing. As reported[1], we prepared libraries for single-cell immune profiling, sequenced and post-processed raw data at the Epigenomics Core at Weill Cornell Medicine.

Sample preparation. To analyse the gene expression of vaccine-induced clones, bulk T cells from patient-derived PBMCs were purified by fluorescence-activated cell sorting and sequenced as previously reported[1]. In brief, we purified single T cells and prepared scRNA-seq libraries as per company specifications prior to performing single-cell immune profiling (10x Genomics, guide CG000330). Each cellular suspension at 97% viability and at 950 cells per μl was loaded onto to a Chromium X to generate Gel Beads-in-Emulsion (GEM) targeting 10,000 single cells per sample.

Sequencing and data processing. To generate 5 P expression libraries, we enzymatically fragmented an aliquot of the cDNA (~50 ng), and end-repaired, A-tailed, subjected to a double-sided size selection with SPRI select beads (Beckman Coulter), and ligated to adaptors. We then introduced a unique sample index for each library through 14 cycles of PCR amplification using the indexes (98 °C for 45 s; 98 °C for 20 s, 54 °C for 30 s and 72 °C for 20 s × 14 cycles; 72 °C for 1 min; held at 4 °C), subjected indexes to a second double-sided size selection, and quantified libraries using Qubit fluorometric quantification (Thermo Fisher Scientific). We assessed quality on an Agilent Bioanalyzer 2100, obtaining an average library size of 460 bp. To generate full-length TCR VDJ regions, we subjected cDNA aliquots (5 ng) to nested PCR amplification with specific VDJ outer and inner primer pairs (98 °C for 45 s; 98 °C for 20 s, 67 °C for 30 s and 72 °C for 20 s × 8 cycles; 72 °C for 1 min; held at 4 °C), 1-sided size selection using SPRI select beads, and assessed quality and quantity of the VDJ region using an Agilent Bioanalyzer 2100. The average library size was 620 bp.

We then clustered gene expression and TCR libraries on an Illumina Novaseq pair end flow cell sequenced for 28-10-10-91, to obtain about 350 million clusters per sample. We processed sequencing images using Illumina's Real Time Analysis software (RTA). We used 10x Genomics Cell Ranger Single Cell Software suite v6.0.0 (https://support.10xgenomics.com/single-cell-gene-expression/software/pipelines/latest/what-is-cell-ranger) to demultiplex, align (hg19), filter, UMI count, and single-cell 5′ end gene count samples, assemble TCRs, annotate paired VDJ, and perform quality control per manufacturer's parameters.

CloneTrack. Clone definition. We defined a T cell clone by the nucleotide CDR3 sequence of the β chain and its V and J genes (TRB). For T cells identified by single-cell sequencing, we defined clones by the CDR3B nucleotide sequence, and mapped clones to paired TCR Vβ sequencing. The V/J genes were disregarded to remove cross-platform biases in V/J gene calling.

We defined the frequency of a clone x as $f_x = \frac{n_x}{N}$, where n_x is the number of reads corresponding to the clone x as defined above, and N is the summation of all productive (in-frame, no stop codons) reads, as done previously[1].

We computed the aggregate frequency of several clones $x \in X$ using an aggregate count $n_X = \sum_{x \in X} n_x$ and used a pseudo-frequency as previously described[1] if $n_X = 0$.

We defined vaccine-induced and atezolizumab (anti-PD-L1)-induced clones as previously described[1]. In brief, in CloneTrack, we select a baseline timepoint, and a time period of interest, and compute P values for each clone to determine if it expands twofold or greater within the determined time period, using a modified Fisher exact test as previously described[1], with Bonferroni multiple hypothesis testing adjustment for both the clones and the number of timepoints examined. We select the most significant timepoint for each clone with an adjusted $P < 0.001$. For vaccine-induced CloneTrack clones, we use the timepoint immediately preceding the vaccine priming dose as the baseline and define the expansion time period to extend until the first dose of chemotherapy (after completing all priming doses). We impose a de novo constraint on prime clones, such that the clones must not be detected in blood before the start of the priming doses. For anti-PD-L1-expanded clones, we use the timepoint immediately preceding the anti-PD-L1 dose as the baseline and define the expansion time period to extend until period immediately after anti-PD-L1. Our updated analyses yield identical clones as detected previously[1].

We defined a clone induced by a vaccine boost by modifying the above described modified Fisher exact test[1] with a twofold expansion factor between the timepoints immediately pre- and post-boost, together with a de novo constraint and a significance threshold of adjusted $P < 0.001$ after accounting for the Bonferroni multiple hypothesis correction. No induced vaccine boost clones were found.

Half-life and lifespan. As we have sufficient timepoints in our CloneTrack time series, we can utilize a standard mathematical method to estimate half-life and lifespan in biological and physical systems—fitting an exponential function to experimentally observed decay rates of individual T cell clones. For each clone, we plot the experimentally measured trajectory (Extended Data Fig. 4e, top), and then derive the half-life and lifespan for the clone after priming doses alone and after priming + boost doses as described below.

(1) To estimate the clone half-life and lifespan post-priming, we identify the peak priming time (time when the clone's frequency peaks before boost), and select all times from peak priming to boost (Extended Data Fig. 4e, top, orange circles).

(2) To estimate the clone half-life and lifespan post-prime/boost, we identify the peak boost time (time of the clone's first measured frequency post-boost), and select all times post peak boost.

When a clone is not detected (frequency = 0), we impute its frequency $f_{\text{imputed}} = 0.5/\text{max\_sample\_norm}$ where max_sample_norm is the total sequence count in the largest sequencing sample in the time series.

We then hypothesize that the frequency of a clone exponentially decays as a function of time:

$$f(t) = f_0 \, e^{-\frac{1}{\tau}(t-t_0)}$$

where $f(t)$ = clone frequency at time t; f_0 = peak clone frequency; τ = mean lifetime. There are two free parameters, $f(t)$ and $t_{1/2}$, which must be inferred. To infer the free parameters for each of these curves, we performed a linear fit on the log of the clone frequencies using a least-square regression (implemented using stats.linregress).

We take $t_0 = 0$ by subtracting peak time from all subsequent times, and linearize the exponential equation:

$$f(t) = f_0 \, e^{-\frac{1}{\tau}(t-t_0)}$$

$$\ln(f(t)) = \ln(f_0) - \frac{1}{\tau}t$$

We can now fit a linear regression to the above equation to derive the decay constant, τ. The fitted slope is $m = -\frac{1}{\tau}$. Therefore:

$$\tau = -\frac{1}{m}$$

As the half-life of a clone is the time for a clone to reduce from its peak frequency by 50%,

$$f(t_{1/2}) = \frac{1}{2} f_0$$

$$t_{1/2} = -\frac{1}{m}\ln(2)$$

Where m is the fitted slope from the observed trajectory.

We define lifespan as time for a clone's frequency to fall below the detection threshold (10^{-6}). We derive the lifespan ($t_{\text{disappearance}}$) as:

$$f(t_{\text{disappearance}}) = f_0 \, e^{-\frac{1}{\tau}t_{\text{disappearance}}}$$

$$10^{-6} = f_0 \, e^{-\frac{1}{\tau}t_{\text{disappearance}}}$$

$$t_{\text{disappearance}} = -\frac{1}{m} \times (\ln(f_0) - \ln(10^{-6}))$$

The two quantities we report from these fits are the half-life ($t_{1/2}$), and the lifespan ($t_{\text{disappearance}}$). These estimated values were then clipped at maximum values of 5 years for the half-life $t_{1/2}$, and 100 years for the disappearance time Δt_d, including for any clones which were growing instead of shrinking, which would infer negative half-lives and lifespan.

To estimate goodness of fit, we calculate the root mean square error (RMSE) that measures for each clone, how far each estimated point is from the observed frequency at that timepoint, averaged across the time series.

Specifically, the RMSE is calculated as

$$\sqrt{\frac{\sum_{i=0}^{N}(y_i' - y_i)^2}{N}}$$

Where N is the number of points being fitted, y_i' is the estimated frequency at timepoint i and y_i is the observed frequency at timepoint i.

We calculate the RMSE in the natural log space in which the equation is fitted and visualize the RMSE (Extended Data Fig. 4e, bottom) on a $\log_{10}$ scale, equivalent to the scale we plot the clone trajectories (Fig. 2b and Extended Data Fig. 2a). All estimated frequencies are within a factor of 10 of the observed frequencies, and 98 of 144 (68%) of estimated frequencies fits lie within a factor of 2 of the observed values.

CloneTrack survival curves. The survival curves of CloneTrack clones were determined based on time from first observation of the clone. As all of these clones were unobserved in the blood pre-vaccination, this appearance time (t_a) can be determined precisely. For the observed survival time (t_s), we took the difference from the last timepoint a clone is observed to the appearance time. For the estimated survival curves we determined the survival time using the disappearance time Δt_d and the start time t_0 (either peak prime frequency or post-boost follow-up time) for that fit:

$$t_s = t_0 + \Delta t_d$$

Note, patient 5 did not receive a boost, so their two CloneTrack clones are included in both the prime and total estimated survival curves.

Time integrated cumulative vaccine frequency. To measure the cumulative frequency of the CloneTrack clones up to a set point in time we computed an integrated average of the aggregate CloneTrack frequency time series. As T cell clone frequencies change on a logarithmic scale, we integrated and averaged the log of the frequency trajectory and then exponentiated at the end (a weighted geometric mean);

$$C(T) = \exp\left(\frac{\int_0^T \log\left(\sum_c p_c(t)\right)dt}{T}\right)$$

Where $p_c(t)$ is the frequency trajectory of CloneTrack clone c. To avoid taking logs of zeros we used a minimum frequency of 2×10^{-6} if no CloneTrack clones were measured at a timepoint. We used a time $t = 644$ days for analysis, corresponding to the latest follow-up timepoint at which complete clonal analysis is available for all patients. The numerical integration was done using scipy.integrate.cumtrapz.

Metaclones. To find additional T cell clones that may be responding to the vaccine, we looked for clonotypes with TCR sequences similar to the vaccine-reactive clones (that is, CloneTrack clones). We used GLIPH2.0[35] with default parameters to cluster all beta chain TCRs (including CDR3 amino acid sequence, V and J gene) of each patient using most available TCR sequencing samples for that patient (restricting samples to early follow-ups). Among the GLIPH groups that were labelled as significant (Fisher score <0.05) compared with the background CD4/CD8 reference TCRs provided by GLIPH2, we identified those containing CloneTrack clones (vaccine-responding metaclones). For each patient, TCR clones (defined by their nucleotide sequence and V/J genes) with CDR3 amino acid sequences belonging to each vaccine-responding metaclone were identified at each timepoint and the sum of the frequencies of these clones (excluding the original CloneTrack clones) was plotted for all available timepoints.

Single-cell analysis. Quality control. Filtered count matrices generated by Cellranger (v6) were integrated into a single matrix using Scanpy[36]. Cells were filtered by having a sequenced high confidence TRB CDR3 region called from Cellranger VDJ (v6). Genes were further filtered based on whether the distribution of the gene expression over the set of cells that express the gene (non-zero expression) has at least 1 nat of entropy and the gene was found in at least 1% of total cells. Both mitochondrial and ribosomal genes were removed.

Phenotyping. Phenotyping was done using the GeneVector pipeline[37]. Cells and genes that pass quality control are embedded according to the GeneVector methodology using mutual information signed by the correlation coefficient into a 20-dimensional latent space[38]. Phenotyping was then done on cells belonging to CloneTrack clones (as

identified by their TRB sequences) by fitting a gaussian mixture model with three components to the cosine similarity of each cell embedding vector onto five genes embedding six vectors (*MKI67*, *GZMB*, *ZNF683* and *KLF2*) as implemented in Scikit-Learn[39].

PhenoTrack. We generated PhenoTrack plots using the phenotyping method described above. Each PhenoTrack plot is defined by examining a set, C, of T cell clones for a particular individual, and tracks the relative frequency, and flow of phenotypes of each clone. As clones can expand or disappear in the repertoire, these plots differ from standard Sankey and alluvial plots in that there is no balanced flow in and out of nodes. To define these plots, we first calculated the frequency of each phenotype f_i for each clone c at each timepoint T, $p_{c,T}(f_i)$). This can be represented as a sum over all cells x that have clonotype c (indicated as $x \sim c$):

$$p_{c,T}(f_i) = \frac{1}{N_T} \sum_{x \in X_T | x \sim c} p(f_i|x)$$

Where X_T is the set of sequenced clones at timepoint T, N_T is the total number of cells in X_T, and $p(f_i|x)$ is the probability cell x has phenotype f_i (if using deterministic assignments this is either 0 or 1). The static phenotype breakdown of each sequenced timepoint can be easily determined by summing over all clones in C:

$$p_{C,T}(f_i) = \sum_{c \in C} p_{c,T}(f_i)$$

This is represented by the solid bars at the sequenced points. We can never determine phenotype swapping of individual cells, as any cell that was sequenced is necessarily not present at the next timepoint, so to determine phenotype flow from one point to the next we examined the phenotype probabilities of clones. It is also important to note that as a clone c may not have the same frequency at timepoint T as at timepoint $T + t$, the total flow out from a timepoint may not equal the flow into the next timepoint. This necessitated us to define both outflow and inflow between adjacent timepoints. The phenotype flow out from a phenotype f_i to f_j for an individual clone c between timepoints T and $T + t$ can be defined according to an independent approximation:

$$\text{outflow}_{c,T \to T+t}(f_i \to f_j) = p_{c,T}(f_i) \times p_{c,T+t}(f_j) \times p_T(c)$$

The inflow for this same transition only differs in the clone frequency normalization:

$$\text{inflow}_{c,T \to T+t}(f_i \to f_j) = p_{c,T}(f_i) \times p_{c,T+t}(f_j) \times p_{T+t}(c)$$

To get the total flows over our clone set C we need only sum over the clones $c \in C$:

$$\text{outflow}_{C,T \to T+t}(f_i \to f_j) = \sum_{c \in C} \text{outflow}_{c,T \to T+t}(f_i \to f_j)$$

and

$$\text{inflow}_{C,T \to T+t}(f_i \to f_j) = \sum_{c \in C} \text{inflow}_{c,T \to T+t}(f_i \to f_j)$$

These outflows and inflows, along with a simple Hill function interpolation between the two, determine the width of the bands showing the transitions between phenotypes. Each band is coloured based on the phenotype it flows out of. Also note, that because a clone may not be present at both timepoints the total flow in/out of a timepoint may not equal the static probabilities, that is:

$$\sum_{f_j} \text{outflow}_{C,T \to T+t}(f_i \to f_j) \le p_{C,T}(f_i)$$

and

$$\sum_{f_i} \text{inflow}_{C,T \to T+t}(f_i \to f_j) \le p_{C,T+t}(f_j)$$

indicating clones either leaving or entering the repertoire at those respective timepoints. For PhenoTrack plots that aggregate over individuals, all of these equations were averaged over the individuals.

We define pre/post-vaccination phases as follows:

- Expansion: all time periods during priming doses of autogene cevumeran
- Contraction: all time periods after priming doses of autogene cevumeran and before mFOLFIRINOX
- Early memory: 0.8–1.8 years post-vaccination
- Mid memory phase: 1.9–2.3 years post-vaccination
- Late memory phase: all time periods from 2.4 years onwards

Ternary plots. The ternary plots were generated by reducing the phenotype space to three phenotypes and determining the phenotype breakdown of each clone of interest only with respect to these phenotypes:

$$f_i(c, T) = \left(\sum_{x \in X_T | x \sim c} p(f_i|x) \right) \Bigg/ \left(\sum_{x \in X_T | x \sim c} \sum_{j=1}^{3} p(f_j|x) \right)$$

These 3D probability vectors can then be plotted on the 2D simplex. Single timepoints can be represented as a scatter plot and transitions between timepoints can be represented by arrows. The width or size of a marker represents the frequency of the clone at the initial timepoint. Clones can also be aggregated together by summing and renormalizing.

P_{gen}. The probability of each amino acid CDR3 TRB to be generated through VDJ recombination, also known as P_{gen}, was computed using the OLGA software[40]. P_{gen} was computed for each TRB in all baseline samples for responding patients using the default human TRB IGoR model[41] shipped with OLGA. Each P_{gen} was computed for the amino acid CDR3 TRB excluding V and J gene restrictions.

Gene-expression analysis. For the differential gene analysis, we specifically examined only cells belonging to CloneTrack clones in patients 1, 6, 10, 11, 14 and 29 (n = 9,110 cells). We normalized the gene expression by the total number of counts in each cell (implemented by scanpy.normalize_total) and computed log gene expression on the normalized genes expression (implemented by scanpy.logp1):

$$\text{LGE}(c, g) = \log(\text{GE}(c, g) + 1)$$

where GE(c,g) is the read count of gene g in cell c.

We computed the differential gene heatmap between phases phase-by-phase. Only genes that were not ribosomal or mitochondrial were considered (n = 24,800). For each phase, we identified genes that were the most significantly upregulated in cells from that phase relative to all other (CloneTrack) cells using Mann–Whitney U with Bonferroni multiple hypothesis correction with an adjusted P value threshold of 0.001. Genes that passed significance were then ordered by their mean differential $\log_2$ gene expression:

$$\text{DLGE}_{\text{Ph}}(g) = \langle \text{LGE}(c, g) \rangle_{c \in \text{Ph}} - \langle \text{LGE}(c, g) \rangle_{c \notin \text{Ph}}$$

where Ph indicates the cells from a particular phase. We depict the top 25 upregulated genes from the phases: expansion, contraction, memory as a heatmap composed of the differential expression for each of these genes at each of the above phases (Fig. 3d).

We generated the gene expression violin plot for a gene g by using the LGE(c,g) of that gene for cells of the labelled phases.

We perform gene set enrichment analysis to confirm genes expressed by vaccine-induced T cells in the expansion phase are modulated by proliferating T cells[42] (gene set: Travaglini_Lung_Proliferating_NK_T_Cell, P value = 2.3×10^{-22}, false discovery rate q value = 3.7×10^{-19}), and in the contraction phase modulated by $CD8^+$ T cells post-antigen exposure (gene set: Kaech_Day8_Eff_VS_Memory_CD8_TCell_DN, P value = 7.8×10^{-18}, false discovery rate q value = 5.4×10^{-15}).

Whole-exome sequencing, mutation identification and phylogeny. We applied the same bioinformatic pipeline as previously described[28]. In brief, we aligned reads to the reference human genome (hg19) using BWA (v0.7.17)[43], and marked duplicates by picard-2.11.0 MarkDuplicates (https://broadinstitute.github.io/picard/). Then, we performed indel realignment by the Genome Analysis toolkit (GenomeAnalysisTK-3.8-1)[44] using RealignerTargetCreator and IndelRealigner. We used the 1000 genome phase1 indel (1000G_phase1.indels.b37.vcf) and Mills indel calls (Mills_and_1000G_gold_standard.indels.b37.vcf) as references. We then calibrated base quality by the GATK's BaseRecalibrator using dbSNP version 138 as reference source. After a pre-processing step, we employed MuTect 1.1.7[45] and Strelka 1.0.15[46] to identify SNVs and indels in tumour samples compared to normal tissue. Using bam-readcounts (v0.8) (https://github.com/genome/bam-readcount), we counted the number of reference and alternative alleles at each mutation position. We then filtered mutations by coverage and variant allele frequency (VAF) by the following criteria: (1) total coverage for tumour ≥10; (2) VAF for tumour ≥4%; (3) number of reads with alternative allele ≥9 for tumour; (4) total coverage for normal ≥7; and (5) VAF for normal ≤1%. After filtering, we took union of filtered mutations within each individual, leveraging primary and recurrent samples. This allowed us to capture coverage and VAF changes from primary to recurrent tumours, even for undetected mutations. We repeated the bam-readcount step for this union set of mutations. Since VAF is not a normalized measure to represent cancer cell fraction (CCF), we used phyloWGS (v1.0-rc2)[47] to reconstruct the phylogeny tree and also to infer CCF on the merged set of mutations. Primary and recurrent tumours share the same topology, but the CCF can differ between primary and recurrent samples. We chose the tree for each sample that has the largest likelihood value. We visualized trees with R package data.tree (v1.1.0) (https://cran.r-project.org/web/packages/data.tree/index.html). The colour represents CCF changes from primary to recurrent tumours in log scale ($\log CCF_{rec}/CCF_{prim}$).

In vitro peptide stimulation. For each neoantigen, we designed 2–4 overlapping 15mer peptides (OLPs, Genscript) covering the mutated neoantigen sequence encoded by the RNA vaccine (Genscript). We resuspended all peptides in DMSO at 10 mg ml^{-1}. Then, we cultured 1×10^6 PBMCs in a 48-well plate with peptide pools (total peptide concentration of 20 μg ml^{-1}) added on day 1, and IL-2 (100 U ml^{-1}) and IL-15 (10 ng ml^{-1}) added on day 2 and every subsequent 2–3 days. Then, on day 7 we restimulated PBMCs with peptide pools, and analysed T cell degranulation by incubating stimulated cells for 1 h with an anti-CD107a antibody, and T cell TNFα and IFNγ production by incubating stimulated cells for 4 h at 37 °C with a protein transport inhibitor (BD Biosciences) and measuring intracellular cytokine production by flow cytometry.

Epitope spreading. To detect epitope spreading in responders, we stimulated PBMCs in vitro with neoantigens not encoded in vaccines. First, we used WES to identify somatic mutations as described above. Then, we filtered out mutations either included in the vaccine, called with low confidence, or whose transcript encoded an amino acid sequence present in the patient reference proteome (that is, we excluded synonymous, stop gain, and start loss mutations). From this set, we computationally created 27mers with the mutated residue at position 14 (where fewer than 13 amino acids were available before or after the mutated residue, all available residues were included), tested binding of 27mer derived 8 to 14mer neoepitopes (excluding all k-mers that did not span the mutation site) to the patient's HLA-I by NetMHCPan4.1, and selected 27mers containing at least one neoepitope predicted to be a strong binder (as per NetMHCPan4.1) or with a binding affinity[27] <150 nM. We then designed 2–4 OLPs (Genscript) covering the mutated 27mer and performed in vitro peptide stimulations of bulk PBMCs as described above.

Flow cytometry and cell sorting. We analysed PBMCs and transduced T cells on a FACS LSR Fortessa (BD Biosciences) using FACSDiva software (version 8.0.1, BD Bioscience). We stained cells for cell surface and intracellular markers using antibody cocktails per manufacturer's recommendations, in a final staining volume of 100 μl, with appropriate controls as indicated. We used the following antibodies and reagents: from BioLegend, CD137 (clone 4B4-1, PE; 3 μl per sample), CD3 (clone SK7, PE-Cy7; 4 μl per sample), CD4 (clone OKT4, Brilliant Violet 650; 2 μl per sample), CD45 (clone 2D1, Alexa Fluor 700; 5 μl per sample), CD56 (clone HCD56, BV605; 2 μl per sample), CD8 (clone SK1, AF700 and APC-Cy7; both 2 μl per sample), HLA_ABC (clone W6/32, APC; 3 μl per sample), IFNγ (clone 4S.B3, BV421; 5 μl per sample), and mTCR (clone H57-597, PE-Cy5; 0.5 μl per sample); from BD Biosciences, CD107a (clone H4A3, PE; 20 μl per sample), CD56 (clone NCAM16.2, BV786; 5 μl per sample), TNFα (clone Mab11, APC; 2.5 μl per sample), and DAPI (564907; 0.2 μl per sample); and from Invitrogen, fixable viability Dye eFluor 520 (65-0867-14; 1.0 μl per sample). We used the following definitions: human T cells as live, $CD45^+CD56^-CD3^+$ cells; degranulating $CD8^+$ T cells as live, $CD56^-CD3^+CD8^+CD107a^+$; neopeptide-stimulated $CD8^+$ T cells as live, $CD56^-CD3^+CD8^+TNFα^+IFNγ^+$; and activated transduced T cells as live, $CD3^+CD8^+mTCR^+4\text{-}1BB^+$. We sorted T cells using an Aria Cell sorter (BD Biosciences). We analysed the data using FlowJo (version 10).

Identification of T cell clones through in vitro neoantigen rechallenge. In vitro neoantigen-specific T cell clones were identified as previously described[1] with minor modifications. In brief, to determine if a T cell clone was specifically stimulated by a neopeptide pool, we sort-purified T cell clones into activated and inactivated fractions ($CD107a^+$ and $CD107a^-$) after peptide stimulation for either TCR Vβ or single-cell VDJ sequencing.

To identify antigen-specific T cell clones, we determined a peptide-specificity stimulation P value for each T cell clone using a one-tailed binomial test (implementing the scipy.stats.binom_test) with a threshold S, to indicate significance with respect to at least S fraction of a clone being antigen-activated. We set the threshold such that no expanded T cell clones were detected in the control (DMSO) PBMCs for the experiment, by sweeping all thresholds from 0 to 1 with steps of 0.1. The minimum threshold which gave no expansion in each DMSO control was selected and an extra step of 0.1 was then added to enforce higher specificity of the expanded clones identified in the experiment. We defined clones based on the nucleotide sequence of the TRB junction. We adjusted P values using Bonferroni correction and determined significance at an adjusted P value threshold of <0.001.

Statistical analyses. Sample sizes (n) represent the number of patients, samples, clones or cells. We analysed survival curves by log-rank (Mantel–Cox) test, compared two groups using unpaired two-tailed Mann–Whitney test, paired groups with two-tailed paired t-test or two-tailed Wilcoxon matched-pairs signed rank test, multiple groups with Kruskal–Wallis test, categorical variables by chi-squared test, and correlated parameters with Spearman correlation. We compared longitudinal clonal expansion by two-tailed Fisher's exact test, and in vitro clonal activation by binomial test with Bonferroni correction. For differential gene-expression analysis, we used Wilcoxon rank sum without any multiple hypothesis correction. $P < 0.05$ was considered statistically significant. All analyses were performed using GraphPad Prism (version 10.1.1) or Python (version 3.11.6).

Reporting summary

Further information on research design is available in the Nature Portfolio Reporting Summary linked to this article.

Data availability

All single-cell sequencing data are available at the Gene Expression Omnibus under accession number GSE222011. All experimental source data are provided. Per institutional data sharing policies, requests for deidentified individual participant data can be made beginning 12 months after publication and for up to 36 months post-publication. Deidentified individual participant data reported in the manuscript will be shared under the terms of a Data Use Agreement that addresses the privacy and security requirements for safeguarding the data under HIPAA and MSK policies, and may only be used for approved proposals. Requests may be made to the corresponding author. Source data are provided with this paper.

Code availability

Code for CloneTrack is available at https://github.com/zsethna/CloneTrack. Code for PhenoTrack is available at https://github.com/zsethna/PhenoTrack. Code to identify GLIPH2 metaclones is available at http://50.255.35.37:8080/tools.

29. Sahin, U. et al. BNT162b2 vaccine induces neutralizing antibodies and poly-specific T cells in humans. *Nature* **595**, 572–577 (2021).
30. Sahin, U. et al. Personalized RNA mutanome vaccines mobilize poly-specific therapeutic immunity against cancer. *Nature* **547**, 222–226 (2017).
31. Holtkamp, S. et al. Modification of antigen-encoding RNA increases stability, translational efficacy, and T-cell stimulatory capacity of dendritic cells. *Blood* **108**, 4009–4017 (2006).
32. Kreiter, S. et al. Mutant MHC class II epitopes drive therapeutic immune responses to cancer. *Nature* **520**, 692–696 (2015).
33. Robins, H. et al. Ultra-sensitive detection of rare T cell clones. *J Immunol Methods* **375**, 14–19 (2012).
34. Carlson, C. S. et al. Using synthetic templates to design an unbiased multiplex PCR assay. *Nat. Commun.* **4**, 2680 (2013).
35. Huang, H., Wang, C., Rubelt, F., Scriba, T. J. & Davis, M. M. Analyzing the Mycobacterium tuberculosis immune response by T-cell receptor clustering with GLIPH2 and genome-wide antigen screening. *Nat. Biotechnol.* **38**, 1194–1202 (2020).
36. Wolf, F. A., Angerer, P. & Theis, F. J. SCANPY: large-scale single-cell gene expression data analysis. *Genome Biol*. **19**, 15 (2018).
37. Ceglia, N. et al. TCRi: Information theoretic metrics for single cell RNA and TCR sequencing in cancer. Preprint at *bioRxiv* https://doi.org/10.1101/2022.10.01.510457 (2022).
38. Ceglia, N. et al. Identification of transcriptional programs using dense vector representations defined by mutual information with GeneVector. *Nat. Commun.* **14**, 4400 (2023).
39. Pedregosa, F. et al. Scikit-learn: machine learning in Python. Preprint at *arXiv* https://doi.org/10.48550/arxiv.1201.0490 (2012).
40. Sethna, Z., Elhanati, Y., Callan, C. G., Walczak, A. M. & Mora, T. OLGA: fast computation of generation probabilities of B- and T-cell receptor amino acid sequences and motifs. *Bioinformatics* **35**, btz035- (2019).
41. Marcou, Q., Mora, T. & Walczak, A. M. High-throughput immune repertoire analysis with IGoR. *Nat. Commun.* **9**, 561 (2018).
42. Travaglini, K. J. et al. A molecular cell atlas of the human lung from single-cell RNA sequencing. *Nature* **587**, 619–625 (2020).
43. Li, H. Aligning sequence reads, clone sequences and assembly contigs with BWA-MEM. Preprint at *arXiv* https://doi.org/10.48550/arxiv.1303.3997 (2013).
44. McKenna, A. et al. The Genome Analysis Toolkit: a MapReduce framework for analyzing next-generation DNA sequencing data. *Genome Res.* **20**, 1297–1303 (2010).
45. Cibulskis, K. et al. Sensitive detection of somatic point mutations in impure and heterogeneous cancer samples. *Nat. Biotechnol.* **31**, 213–219 (2013).
46. Saunders, C. T. et al. Strelka: accurate somatic small-variant calling from sequenced tumor–normal sample pairs. *Bioinformatics* **28**, 1811–1817 (2012).
47. Deshwar, A. G. et al. PhyloWGS: reconstructing subclonal composition and evolution from whole-genome sequencing of tumors. *Genome Biol*. **16**, 35 (2015).

Acknowledgements The authors thank patients and their families for partaking in this clinical trial and for donating tissues for research. We acknowledge all the clinical research staff of the Hepatopancreatobiliary Service, the Precision Pathology Biobanking Center, and the Center for Molecular Oncology at MSK. This work was supported in part by The Olayan Charitable Foundation and The Tow Foundation, and by a Stand Up to Cancer Convergence Award (to B.D.G. and V.P.B.), the NIH U01 CA224175 Pancreatic Cancer Microenvironment Network Cancer Moonshot Award (to V.P.B.), the Ben and Rose Cole Charitable PRIA Foundation (to V.P.B), the Mark Foundation ASPIRE Award (to B.D.G.), William H. Goodwin and Alice Goodwin and the Commonwealth Foundation for Cancer Research and The Center for Experimental Therapeutics at MSK (to V.P.B. and B.D.G.), the Center for Experimental Immuno-Oncology of MSK (to P.G.) and the American-Italian Cancer Foundation Post-Doctoral Research Fellowship (to M.M.). Services of the Integrated Genomics Core were funded by the NCI Cancer Center Support Grant (CCSG, P30 CA08748), Cycle for Survival and the Marie-Josée and Henry R. Kravis Center for Molecular Oncology. The team at MSK sponsored the clinical trial. The project was supported by the imCORE Network, Genentech, BioNTech, Stand Up To Cancer, the Lustgarten Foundation and the National Cancer Institute Pancreatic Cancer Microenvironment Network.

Author contributions Author contributions (including J.D.W., T.M., N.P., O.B., A.S.E., P.M., W.P., R.S., A.M.V., E.W., A.D., A.C.W., M.I.D., T.P.K., K.C.S., J.D. and W.R.J.) to the clinical trial are previously reported[1]. Z.S. and M.M. performed all clonal computational analyses. P.G. and C.R. performed all immunologic assays with assistance from G.P., L.A.R., A.O., M.A., A.Z., Z.O., E.M.B., S.L.Z. and C.C. Z.S. and N.C. performed all single-cell analyses. J.L. and Z.S. performed the clone reconstructions and phylogeny. M.M., O.L. and Y.E. performed metaclone analyses. The BioNTech team (E.D., F.M., L.M., U.S. and Ö.T.), coordinated by F.M., selected the neoantigens, designed and manufactured the individualized mRNA vaccines. M.G. provided statistical oversight. V.P.B. and E.M.O. oversaw all aspects of clinical trial conduct as primary and co-primary investigators, respectively. B.D.G. supervised the computational work. All data were collected and analysed at MSK, with interpretation and critical feedback from all authors (Z.S., P.G., C.R., M.M., N.C., E.P., J.L., G.P., O.L., L.A.R., N.P., A.O., M.A., A.Z., Z.O., E.M.B., S.L.Z., C.C., Y.E., E.D., L.M., F.M., I.R., M.Y., T.M., J.D.W., O.B., M.G., A.S.E., P.M., W.P., R.S., A.M.V., E.W., A.D., A.C.W., M.I.D., T.P.K., K.C.S., W.R.J., J.D., E.M.O., I.M., U.S., Ö.T., B.D.G., and V.P.B.). Z.S., P.G., C.R., M.M., E.P., E.D., L.M., F.M., I.R., M.Y., I.M., U.S., Ö.T., B.D.G. and V.P.B. participated in critical discussions and manuscript writing. B.D.G. supervised the computational work. V.P.B. supervised and coordinated all aspects of the project. The funders had no role in the conduct of the trial or endpoint analyses. The authors assume responsibility for the completeness and accuracy of the data and for the fidelity of the trial to the protocol and statistical analysis plan.

Competing interests L.A.R., Z.M.S., B.D.G. and V.P.B. are inventors on patent applications related to work on antigen cross-reactivity and tracking vaccine-induced T cell clones. B.D.G. and V.P.B. are inventors on a patent application on neoantigen quality modelling. L.A.R. is an inventor of a patent related to oncolytic viral therapy. B.D.G. has received honoraria for speaking engagements from Merck, Bristol Meyers Squibb and Chugai Pharmaceuticals; has received research funding from Bristol Meyers Squibb, Merck and ROME Therapeutics; and has been a compensated consultant for Darwin Health, Merck, PMV Pharma, Shennon Biotechnologies, Synteny and Rome Therapeutics of which he is a co-founder. V.P.B. reports honoraria and research support from Genentech and research support from Bristol-Myers Squibb. A.S.E received royalties from Up-To-Date. A.V. reports research funding from Lilly, Verastem, BioMed Valley Discoveries, Bristol-Myers Squibb and Silenseed. A.C.W. reports the following: Histosonics, consulting and Ipsen, clinical trial funding. E.M.O. reports research funding to the institution from: Genentech/Roche, BioNTech, AstraZeneca, Arcus, Elicio, Parker Institute, NIH/NCI, Digestive Care and Break Through Cancer; consulting via Data and Safety Monitoring Board (DSMB) for: Arcus, Alligator, Agenus, BioNTech, Ipsen, Merck, Moma Therapeutics, Novartis, Syros, Leap Therapeutics, Astellas, BMS, Fibrogen, Revolution Medicine, Merus Agios (spouse), Genentech-Roche (spouse), Eisai (spouse) and Servier (Spouse). J.D. owns stock in Alnylam Pharmaceuticals, Arrowroot Acquisition and Ionis Pharmaceuticals. T.M. is a co-founder and holds equity in IMVAQ Therapeutics; is a consultant for Immunos Therapeutics, ImmunoGenesis and Pfizer; has research support from Bristol-Myers Squibb, Surface Oncology, Kyn Therapeutics, Infinity Pharmaceuticals, Peregrine Pharmaceuticals, Adaptive Biotechnologies, Leap Therapeutics and Aprea; and has patents on applications related to work on oncolytic viral therapy, alphavirus-based vaccine, neoantigen modelling, CD40, GITR, OX40, PD-1 and CTLA-4. J.D.W. is a consultant for Apricity, CellCarta, Ascentage Pharma, AstraZeneca, Bicara Therapeutics, Boehringer Ingelheim, Bristol-Myers Squibb, Daiichi Sankyo, Dragonfly, Georgiamune, Imvaq, Larkspur, Psioxus, Recepta, Tizona and Sellas. J.D.W. receives grant and research support from Bristol-Myers Squibb and Sephora. J.D.W. has equity in Apricity, Arsenal IO, Ascentage, Imvaq, Linneaus, Georgiamune, Maverick and Tizona Therapeutics. W.P. reports research funding to institution from: Merck, Astellas, Miracogen and Amgen; consultancy or advisory board activity for: Astellas and EXACT Therapeutics; honoraria for Continuing Medical Education (CME) from: American Physician Institute and Integrity. O.T. and U.S. are co-founders, management board members and employees at BioNTech. E.D., L.M. and F.M. are employees at BioNTech. I.R., M.Y. and I.M. are employees at Genentech. The other authors declare no competing interests.

Additional information

Supplementary information The online version contains supplementary material available at https://doi.org/10.1038/s41586-024-08508-4.

Correspondence and requests for materials should be addressed to Vinod P. Balachandran.

Peer review information *Nature* thanks Robert Seder, Neeha Zaidi and the other, anonymous, reviewer(s) for their contribution to the peer review of this work.

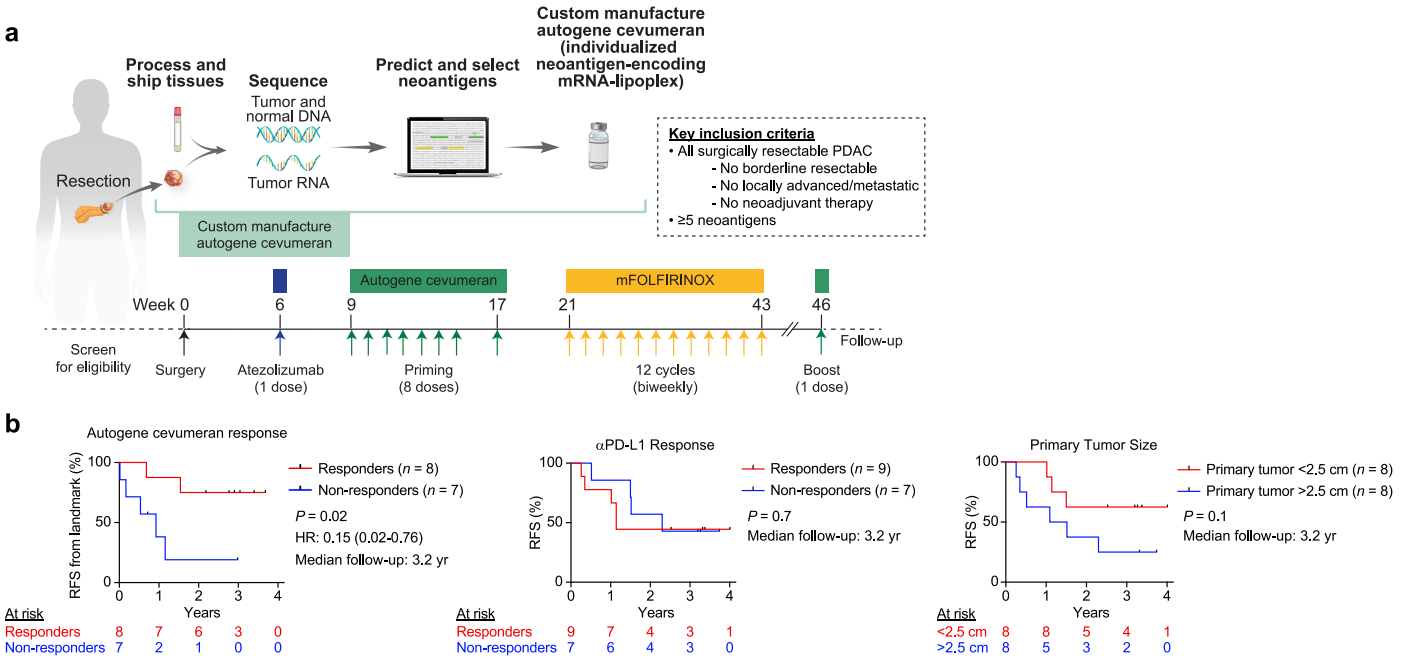

Extended Data Fig. 1 | Autogene cevumeran but not atezolizumab response or tumor size correlates with RFS at 3-year follow-up. a, Trial schematic as previously reported[1]. Reproduced under CC BY 4.0: https://creativecommons.org/licenses/by/4.0/. **b**, Recurrence-free survival (RFS) from landmark time (last vaccine priming dose) stratified by autogene cevumeran (vaccine) immunologic response determined by ex vivo IFNγ ELISpot[1] (**left**), and RFS from surgery stratified by anti-PD-L1 (atezolizumab) response (**middle**) and median primary tumour size (**right**). HR, hazard ratio with 95% confidence interval. Black tick marks, censorship points. *n* is the number of individual patients. *P* values by two-tailed log-rank test (**b**).

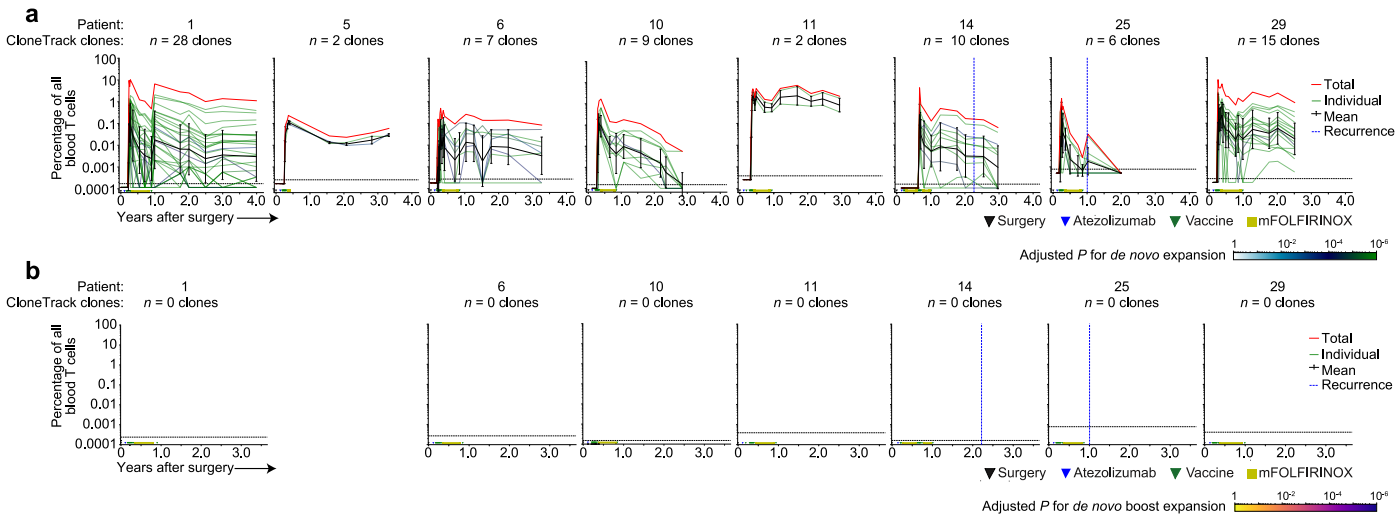

Extended Data Fig. 2 | Autogene cevumeran induces de novo T cell clones at prime but not boost. a, b, Vaccine-induced T cell clones at prime (**a**) and boost (**b**) identified by CloneTrack. Patient 5 did not receive boost dose and is excluded from (**b**). Black, blue, green, yellow symbols indicate surgery, atezolizumab, vaccination, mFOLFIRINOX times, respectively. Horizontal line, clone detection threshold; vertical line, recurrence time. Line colour indicates adjusted *P* value for de novo expansion. *n* is the number of clones. *P* values by modified two-tailed Fisher's exact test (**a, b**).

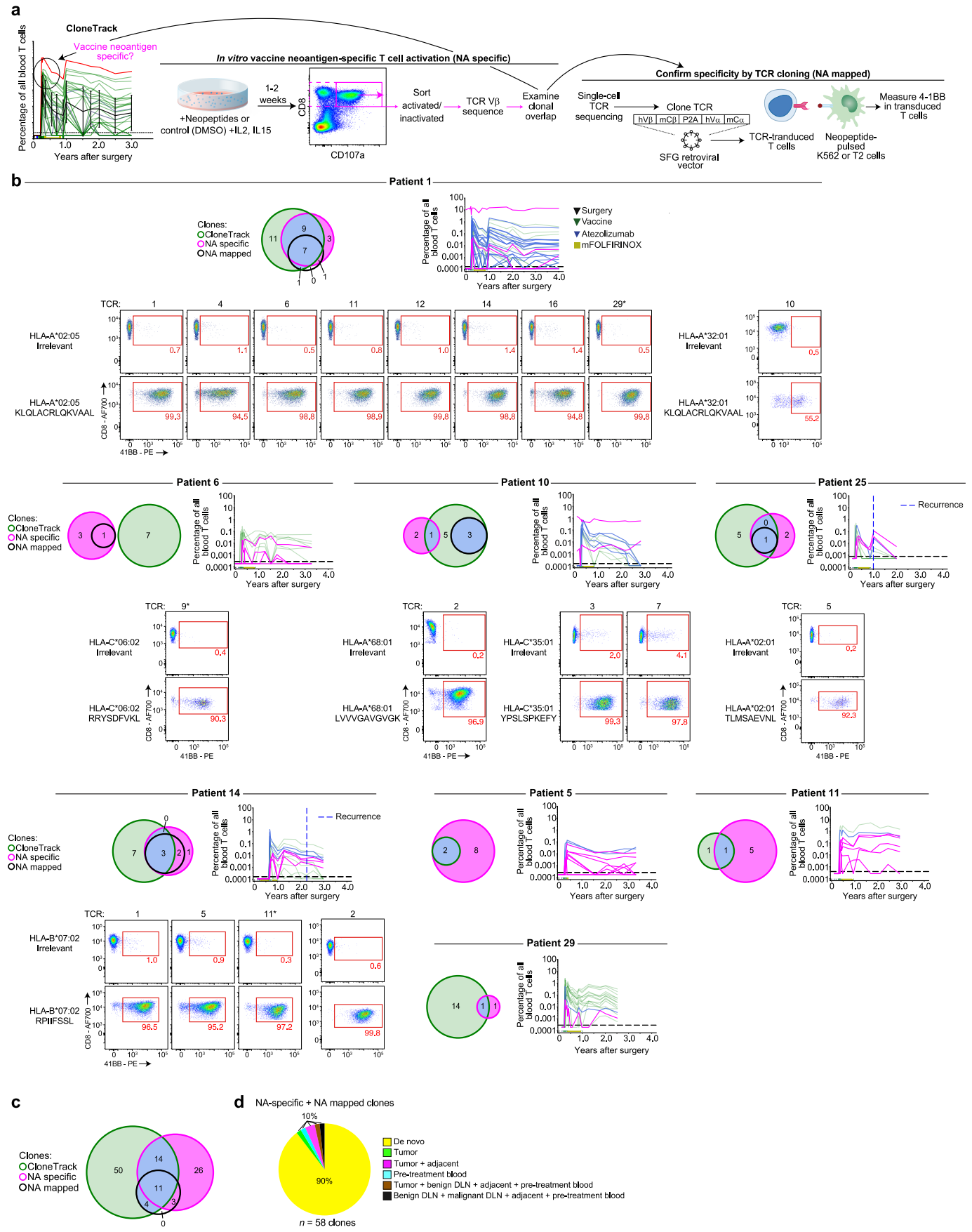

Extended Data Fig. 3 | See next page for caption.

Extended Data Fig. 3 | Autogene cevumeran-induced clones identified by CloneTrack contain neoantigen-specific clones. a-d, To identify neoantigen-specific T cell clones, we stimulated PBMCs at various timepoints post-vaccination in vitro with overlapping neopeptide pools. We then purified $CD8^+CD107a^{+/-}$ T cells and identified clones with greater proportion of activated ($CD107a^+$) versus inactivated ($CD107a^-$) cells as in vitro neoantigen-specific T cell clones (NA specific) (as done previously[1]; **Methods**). For select clones and patients, we validated neoepitope specificity by TCR cloning (NA mapped). **a**, Assay schematic. **b**,**c**, Venn diagrams show overlap of CloneTrack clones (green Venn), NA-specific clones (clones identified as neoantigen-specific with in vitro vaccine neoantigen-specific T cell activation as in **a**, pink Venn) and NA-mapped clones (clones mapped to neoepitopes by TCR cloning as in **a**, black Venn) in individual (**b**) and all (**c**) $n = 8$ responders. Trajectory plots/Venn shading show in vivo longitudinal expansion/contraction of clones identified by CloneTrack and validated experimentally (blue shading in Venn diagrams), identified by CloneTrack but not experimentally validated (green shading in the Venn diagrams), and experimentally validated but not found by CloneTrack (pink shading in Venn diagrams). Flow cytometry (**b**) shows 4-1BB expression on neoantigen-specific TCR-transduced $CD8^+$ T cells (identified as in **a**, NA mapped clones) cultured with HLA-matched, neo or irrelevant peptide-pulsed antigen-presenting cells. Cells were gated on live, $CD3^+CD8^+$ TCR-transduced cells. * Denotes $CloneTrack^-$ clones. (**d**) Percentage of NA-specific and NA-mapped clones (as in **c**) contained in tissues. Black, blue, green, and yellow symbols indicate surgery, atezolizumab, vaccination, and mFOLFIRINOX times, respectively. *n* is the number of clones.

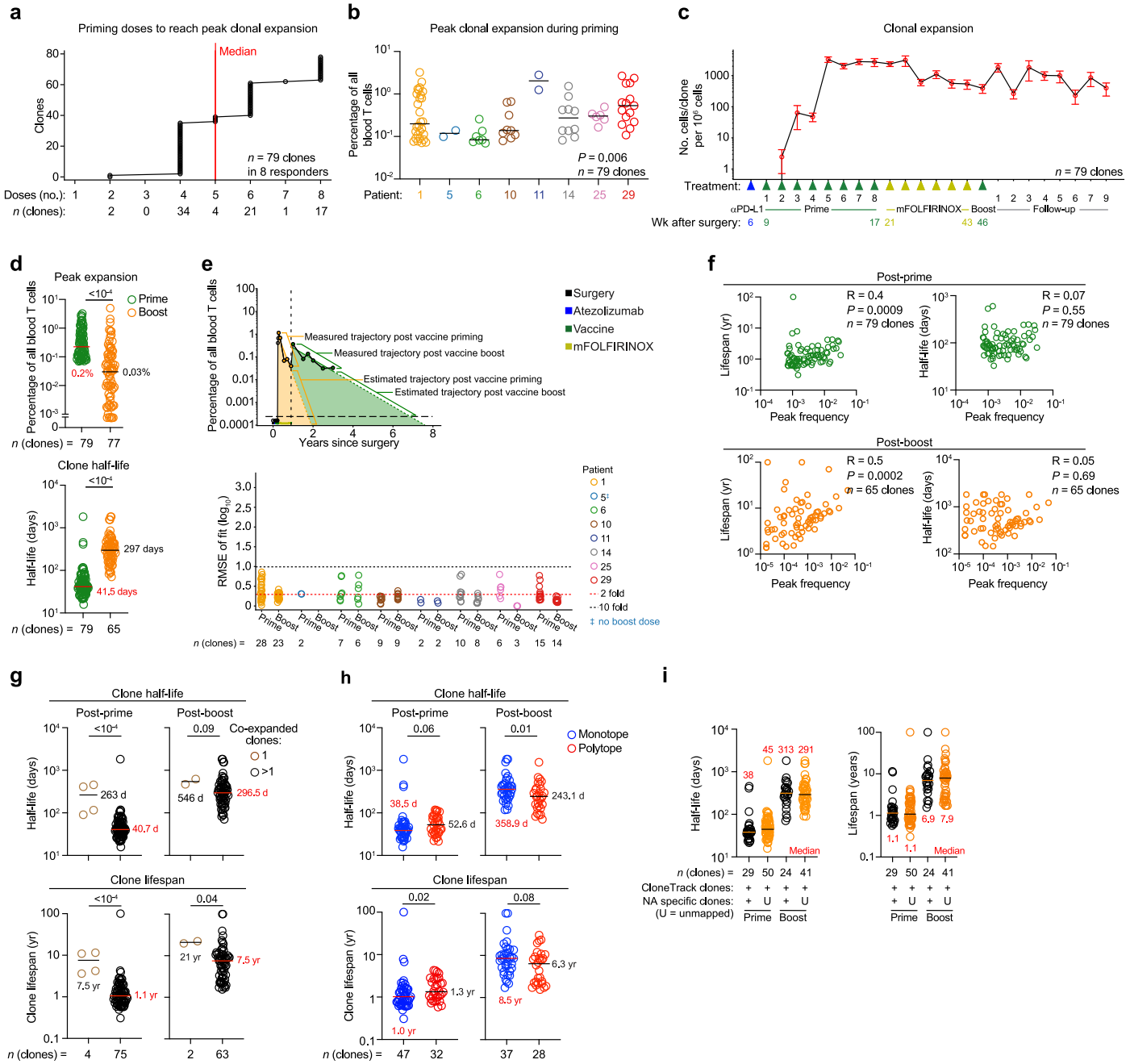

Extended Data Fig. 4 | Dynamics, half-lifes and lifespans of autogene cevumeran-induced CloneTrack clones. a, Number of autogene cevumeran priming doses for CloneTrack clones (identified as in Extended Data Fig. 2a) to reach peak expansion in blood. Red line, median doses to reach peak expansion. **b**, Percentage of individual patient T cell repertoires represented by individual CloneTrack clones at peak expansion in (**a**). **c**, Longitudinal average number of all CloneTrack clone cells per million T cells in responders ($n = 8$) over time. Circles, mean; error bars, s.e.m. **d**, Peak expansion (**top**) and half-life (**bottom**) of CloneTrack clones post-prime and boost. **e**, (**Top**) Representative estimated trajectories post vaccine prime and boost. (**Bottom**) Root mean square error (RMSE) of exponential fits of estimated trajectories for each clone in each patient. Dashed lines denote where average estimated differences between observed and estimated measurements vary by a factor of 2 (**red**) or 10 (**black**). **f**, Correlation of vaccine-induced expansion peak frequency post-prime (**top**) and post-boost (**bottom**) with estimated lifespan (**left**) and half-life (**right**). **g**, CloneTrack clone half-life (**top**) and lifespan (**bottom**) with one or more co-expanded clones post-prime (**left**) and boost (**right**). **h**, CloneTrack clone half-life (**top**) and lifespan (**bottom**) post-prime (**left**) and boost (**right**) in monotope and polytope responders. **i**, Lifespan of CloneTrack clones stratified by mapped/unmapped neoantigen (NA) specificity in vitro (as in Extended Data Fig. 3a–c). In **d**-**h**, $n = 8$ patients post-prime and $n = 7$ patients post-boost (patient 5 no boost). n is the number of clones. P values by Kruskal-Wallis test (**b**), two-tailed Mann Whitney test (**d**, **g**, **h**) and two-tailed Spearman correlation (**f**).

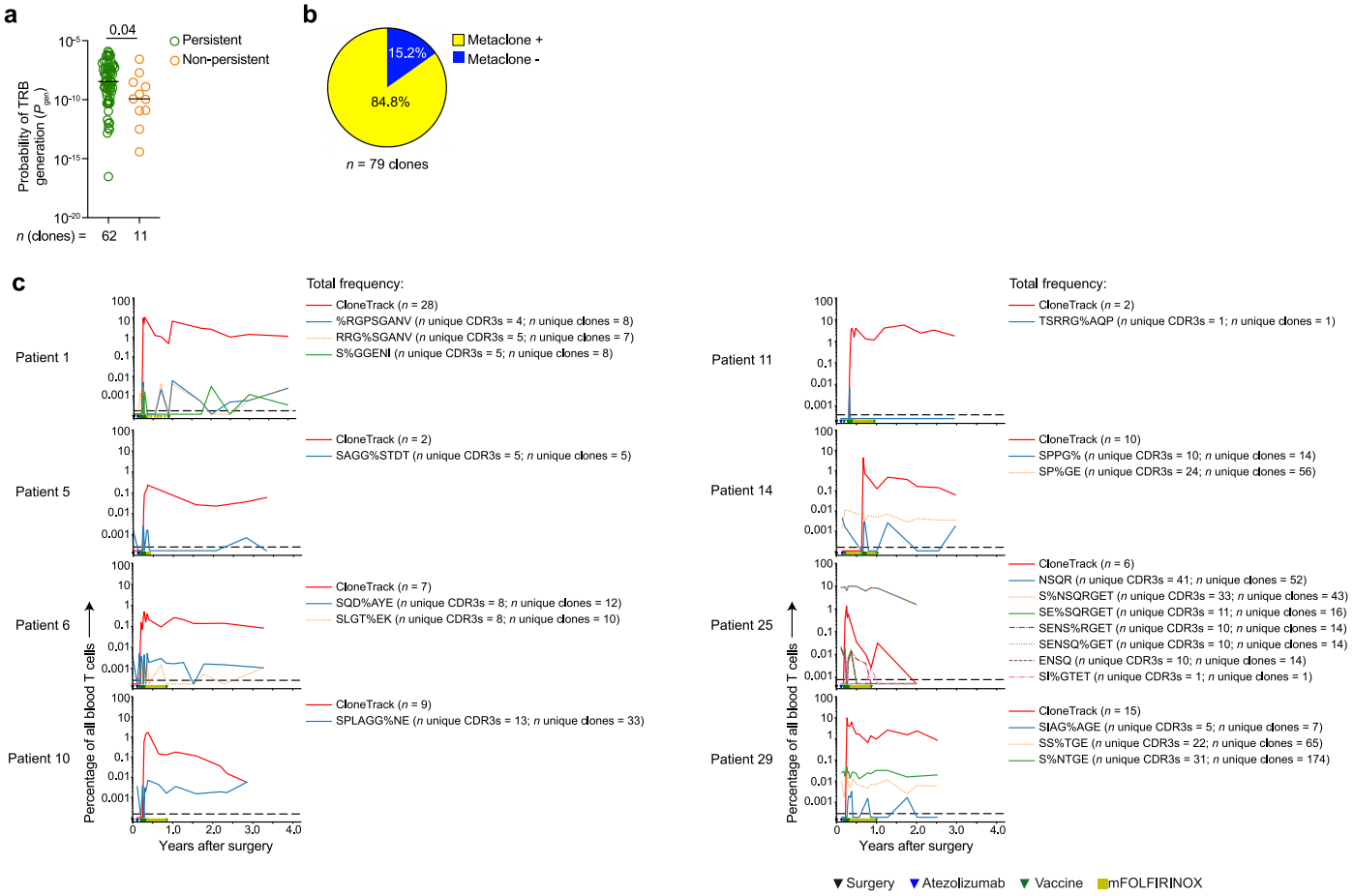

Extended Data Fig. 5 | T cell clones in shared TCR Vβ specificity groups do not co-expand with autogene cevumeran-induced CloneTrack clones. **a**, Generation probability (P_{gen}) of CloneTrack clones that do/do not persist >2 years post-vaccination (persistent/non-persistent). **b**, Percentage of CloneTrack clones with intra-patient metaclones in shared TCR Vβ specificity groups. Metaclones were identified as clonotypes with TCR sequences similar to the vaccine-reactive clones (i.e., CloneTrack clones) using GLIPH2.0[35]. **c**, Individual longitudinal trajectories of CloneTrack metaclones and aggregate CloneTrack clones for comparison. Black, blue, green, and yellow symbols indicate surgery, atezolizumab, vaccination, and mFOLFIRINOX times, respectively. *n* is the number of clones. *P* value by two-tailed Mann Whitney test (**a**).

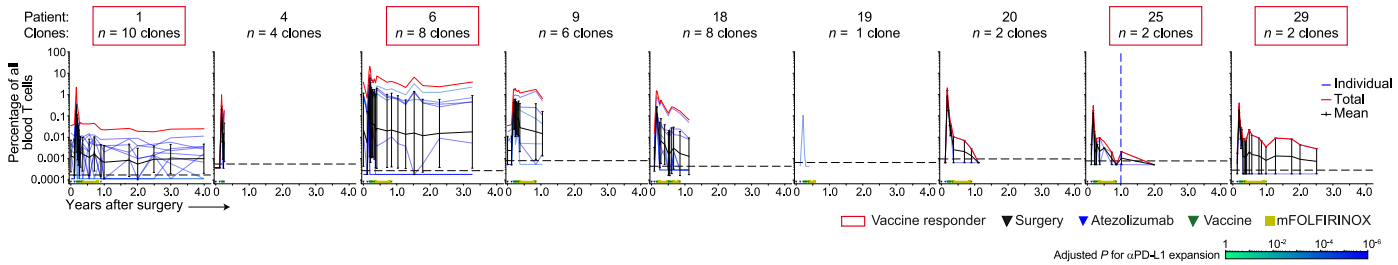

Extended Data Fig. 6 | Dynamics of atezolizumab-induced T cell clones. **a**, Atezolizumab (anti-PD-L1)-induced T cell clones identified by CloneTrack in all vaccine responders. Horizontal line, clone detection threshold; red box, autogene cevumeran responders. Black, blue, green, and yellow indicate surgery, atezolizumab, vaccination and mFOLFIRINOX times, respectively. *n* is the number of clones. *P* values by modified two-tailed Fisher's exact test.

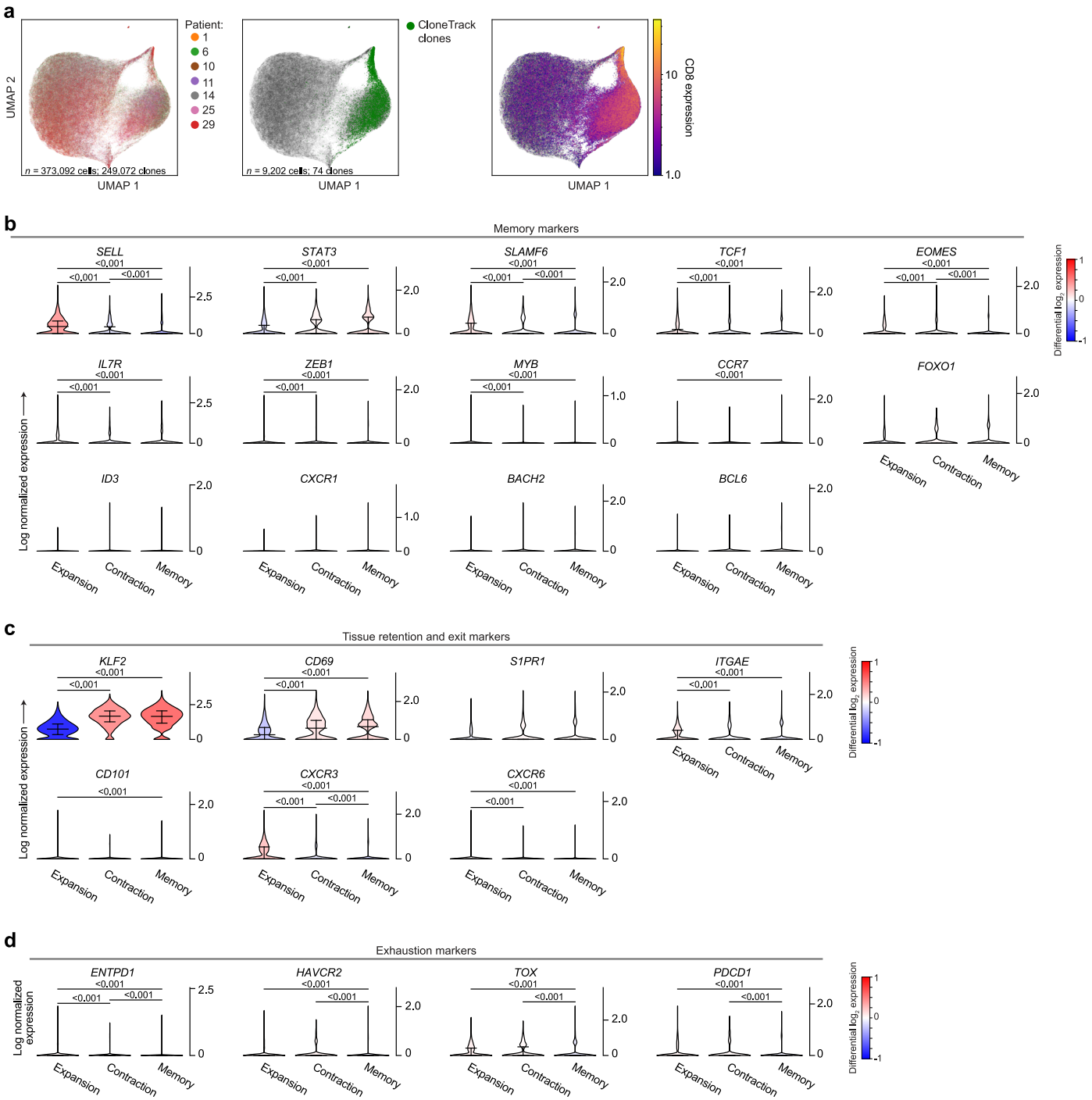

Extended Data Fig. 7 | Autogene cevumeran-induced CloneTrack clone T cells do not acquire exhaustion features long-term. a, UMAPs of single-cell RNA and TCR sequencing of all blood T cells (all patients, all times) stratified by patient (**left**), CloneTrack clones (**middle**) and CD8 expression (**right**). **b-d**, Violin plots of select central/effector memory (**b**), tissue retention (**c**) and T cell exhaustion (**d**) associated genes in CloneTrack clone T cells at expansion, contraction and memory phases by single-cell RNA/TCR sequencing as shown in Fig. 3a. *n* is the number of cells or clones. *P* values by two-sided pairwise Wilcoxon rank sum test.

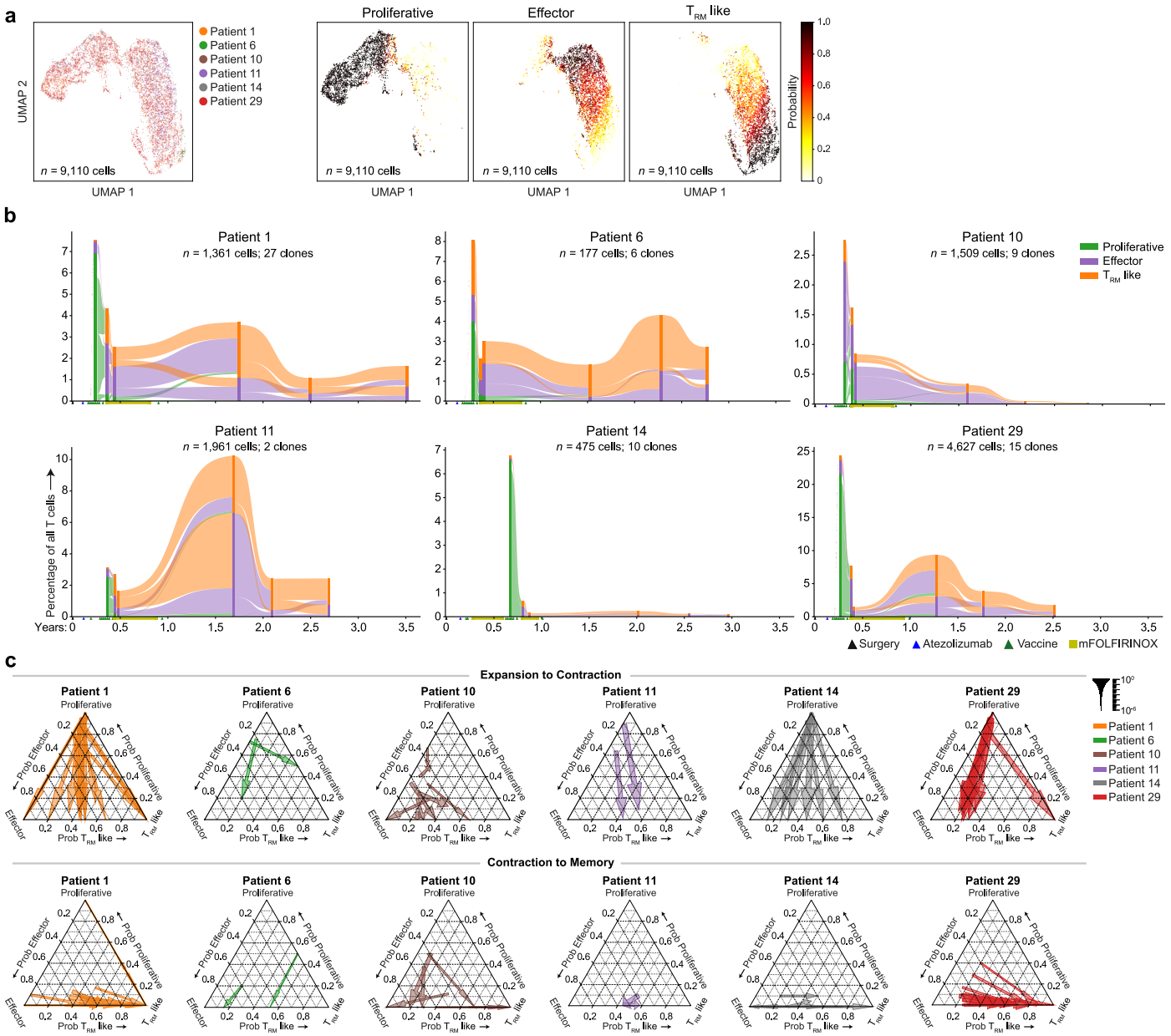

Extended Data Fig. 8 | Autogene cevumeran-induced CloneTrack clones retain an effector phenotype despite post-vaccination chemotherapy. **a**, UMAPs of single-cell RNA and TCR sequencing of CloneTrack clone T cells (all patients, all times) stratified by patient (**left**) and phenotype (**right**). **b**, PhenoTrack plots of phenotype composition and conversion of CloneTrack clones over time in individual responders. Vertical coloured bars show the proportion of cells of each phenotype at corresponding times. Black, blue, green and yellow rectangles indicate surgery, atezolizumab, vaccination and mFOLFIRINOX times, respectively. **c**, Phenotype conversion of CloneTrack clones from expansion to contraction (**top**) and contraction to memory (**bottom**) phases in individual responders. Arrows, individual clones; axis proximity of arrow base, fraction of cells per clone in a phenotype; arrows point from phenotype origin to destination; arrow width, clone frequency. *n* is the number of cells.

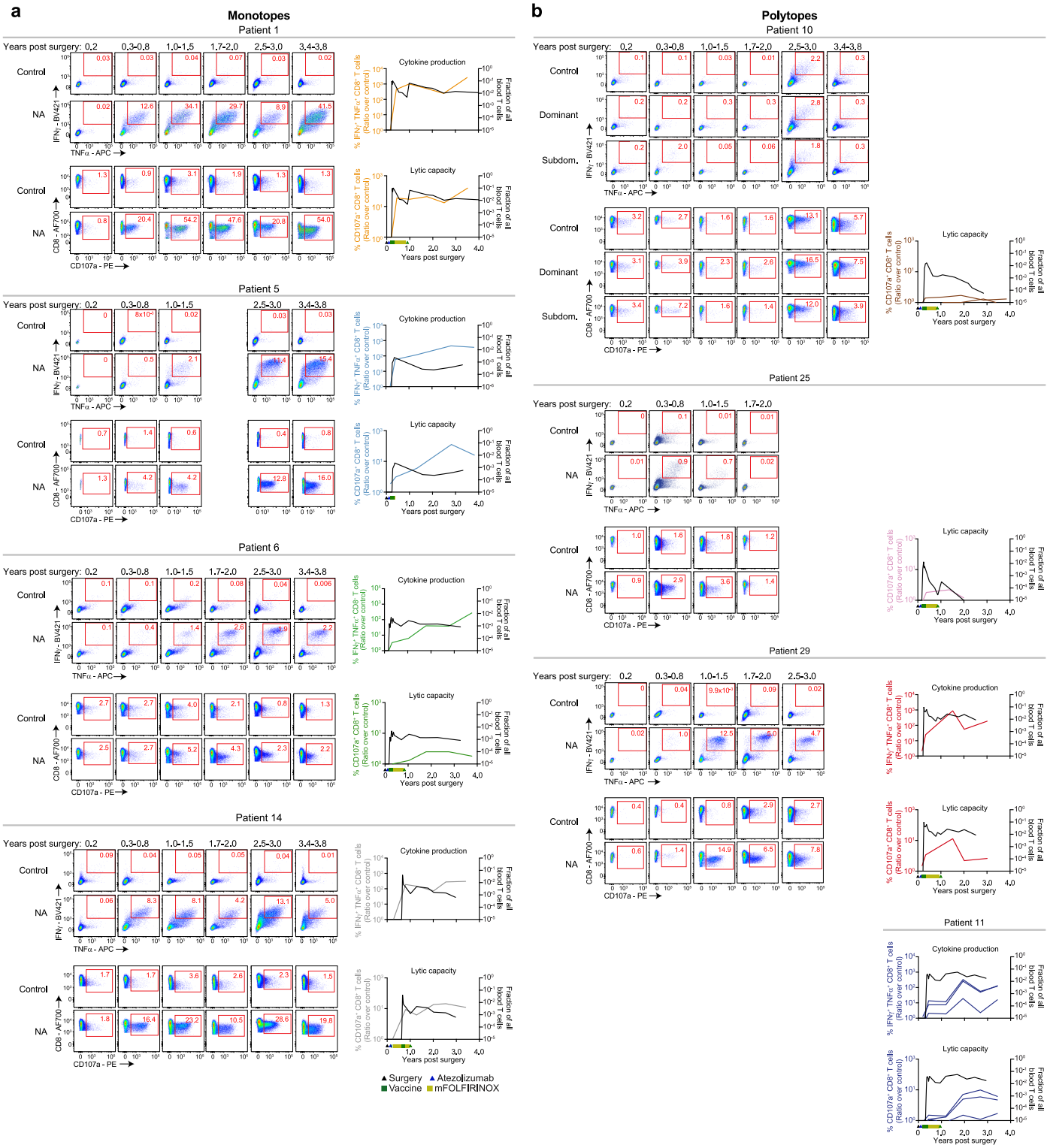

Extended Data Fig. 9 | Autogene cevumeran-induced CloneTrack clone frequency correlates with neoantigen-specific functional recall in vitro. **a, b,** Longitudinal cytokine production and lytic capacity (flow cytometry, left; colored curves, right) of CD8$^+$ T cells post bulk PBMC in vitro rechallenge with immunodominant and sub-dominant ELISpot$^+$ vaccine neoantigens, and aggregate fraction of autogene cevumeran-induced CloneTrack clones (black curves) in monotope (**a**) and polytope (**b**) responders. Flow cytometry is gated on live, CD3$^+$CD56$^-$CD8$^+$ cells. Data for patients 10, 25 (cytokine production) and 11 (flow cytometry) are in Fig. 4a,b.

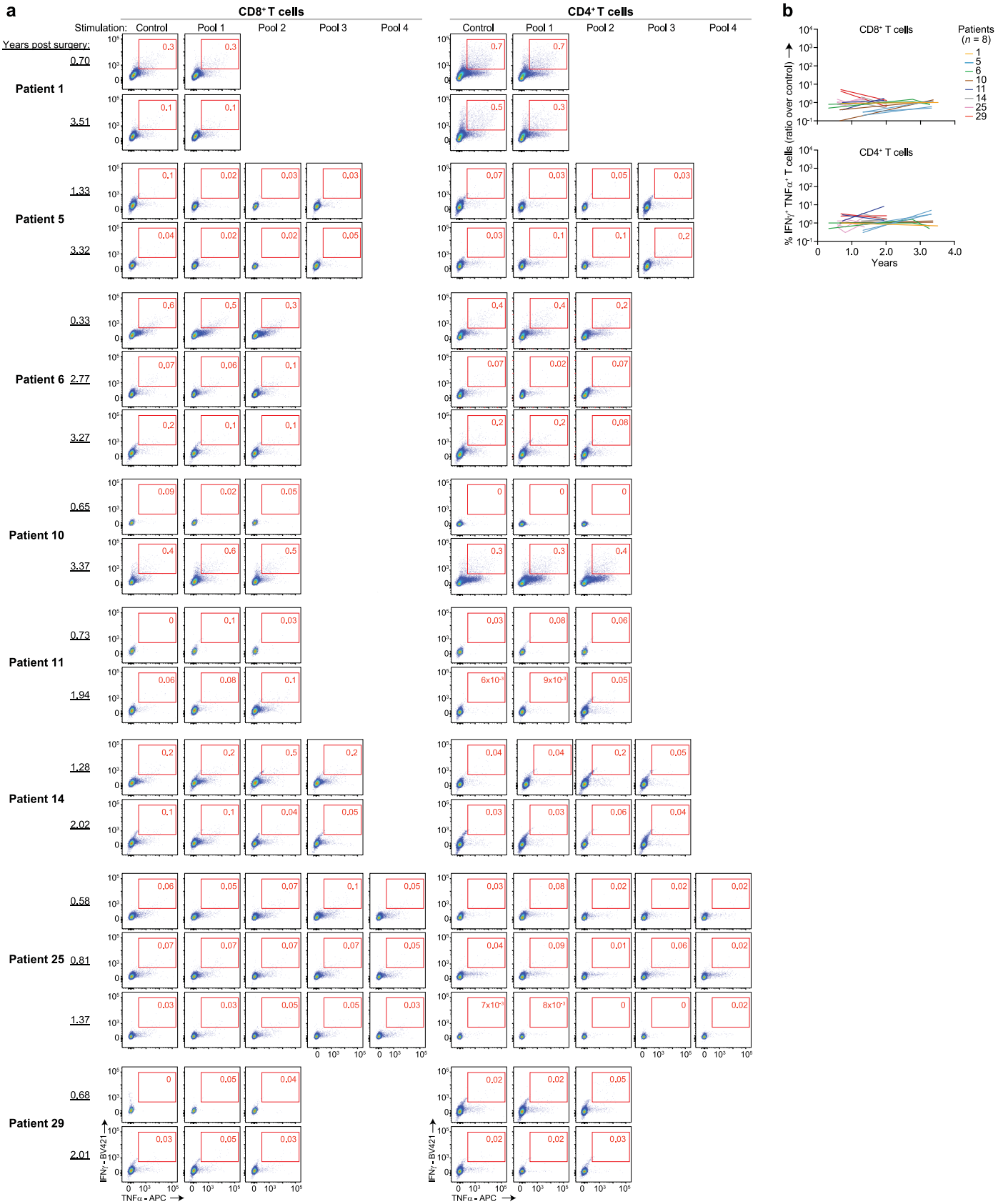

Extended Data Fig. 10 | Autogene cevumeran responders do not acquire immune activity against non-vaccine neoantigens. a, b, Longitudinal cytokine production of CD8$^+$ and CD4$^+$ T cells post bulk PBMC in vitro rechallenge with pools of non-vaccine tumor neoantigens depicting individual (**a,** flow cytometry) and aggregated (**b**) data in responders. Flow cytometry is gated on live, CD3$^+$CD56$^-$CD8$^+$ cells (**left**) and on live, CD3$^+$CD56$^-$CD4$^+$ cells (**right**).

nature portfolio

Corresponding author(s): Vinod Balachandran

Last updated by author(s): Nov 12, 2024

Reporting Summary

Nature Portfolio wishes to improve the reproducibility of the work that we publish. This form provides structure for consistency and transparency in reporting. For further information on Nature Portfolio policies, see our Editorial Policies and the Editorial Policy Checklist.

Statistics

For all statistical analyses, confirm that the following items are present in the figure legend, table legend, main text, or Methods section.

n/a	Confirmed
☐	☒ The exact sample size (*n*) for each experimental group/condition, given as a discrete number and unit of measurement
☐	☒ A statement on whether measurements were taken from distinct samples or whether the same sample was measured repeatedly
☐	☒ The statistical test(s) used AND whether they are one- or two-sided *Only common tests should be described solely by name; describe more complex techniques in the Methods section.*
☐	☒ A description of all covariates tested
☐	☒ A description of any assumptions or corrections, such as tests of normality and adjustment for multiple comparisons
☐	☒ A full description of the statistical parameters including central tendency (e.g. means) or other basic estimates (e.g. regression coefficient) AND variation (e.g. standard deviation) or associated estimates of uncertainty (e.g. confidence intervals)
☐	☒ For null hypothesis testing, the test statistic (e.g. *F*, *t*, *r*) with confidence intervals, effect sizes, degrees of freedom and *P* value noted *Give P values as exact values whenever suitable.*
☒	☐ For Bayesian analysis, information on the choice of priors and Markov chain Monte Carlo settings
☒	☐ For hierarchical and complex designs, identification of the appropriate level for tests and full reporting of outcomes
☐	☒ Estimates of effect sizes (e.g. Cohen's *d*, Pearson's *r*), indicating how they were calculated

Our web collection on statistics for biologists contains articles on many of the points above.

Software and code

Policy information about availability of computer code

Data collection

TCR Vβ sequencing – We used Dropsense 96 to quantify samples, dilute standard concentrations, and prepare libraries. We then generated sample data using an immunoSEQ Assay (Adaptive Biotechnologies).

Single cell RNA/TCR sequencing – We assessed the quality of PCR amplifications on an Agilent Bioanalyzer 2100. Pooled libraries were clusteredon an Illumina Novaseq pair end flow cell sequenced for 656 28-10-10-91, to obtain about 350 million clusters per sample. We processed sequencing images using Illumina's Real Time Analysis software (RTA). We used 10x Genomics Cell Ranger Single Cell Software suite v6.0.0 to demultiplex, align (hg19), filter, UMI count, and single-cell 5' end gene count samples, assemble TCRs, annotate paired VDJ, and perform quality control per manufacturer's parameters.

Flow cytometry and cell sorting – We analyzed PBMCs, transduced cells, and activated T cells on a FACS LSR Fortessa (BD Biosciences) using FACSDiva software (version 8.0.1, BD Bioscience). We sorted cells using and Aria Cell sorter (BD Biosciences).

Data analysis

All analyses were performed using GraphPad Prism (version 10.1.1) or Python (version 3.11.6).

Flow cytometry – We analyzed data using FlowJo (version 10).

Time integrated cumulative vaccine frequency – The numerical integration was done using scipy.integrate.cumtrapz.

Analysis of metaclones – We used GLIPH2.0.

Single cell analysis – We performed quality control by filtering count matrices generated by Cellranger (v6) and integrating them into a single

matrix using Scanpy. Cells were filtered by having a sequenced high confidence TRB CDR3 region called from Cellranger VDJ (v6). Phenotyping was done using the GeneVector pipeline.

Whole exome sequencing, mutation identification, and phylogeny – we aligned reads to the reference human genome (hg19) using BWA (v0.7.17), and marked duplicates by picard-2.11.0 MarkDuplicates. Then, we performed indel realignment by the Genome Analysis toolkit (GenomeAnalysisTK-3.8-1)44 using RealignerTargetCreator and IndelRealigner. We used the 1000 genome phase1 indel (1000G_phase1.indels.b37.vcf) and Mills indel calls (Mills_and_1000G_gold_standard.indels.b37.vcf) as references. We then calibrated base quality by the GATK's BaseRecalibrator using dbSNP version 138 as reference source. After a pre-processing step, we employed MuTect 1.1.745 and Strelka 1.0.1546 to identify SNVs and indels in tumor samples compared to normal. Using bam-readcounts (v0.8). We used phyloWGS (v1.0-rc2) to reconstruct the phylogeny tree and also to infer CCF on the merged set of mutations. We visualized trees with R package data.tree (v1.1.0).

Predicted HLA-I binding affinity – We used NetMHCPan4.1.

Analyses of TCR Vβ sequencing and single cell RNA/TCR sequencing data used custom code:
Code for CloneTrack is available at https://github.com/zsethna/CloneTrack
Code for PhenoTrack is available at https://github.com/zsethna/PhenoTrack
Code to identify GLIPH 2 metaclones is available at http://50.255.35.37:8080/tools

For manuscripts utilizing custom algorithms or software that are central to the research but not yet described in published literature, software must be made available to editors and reviewers. We strongly encourage code deposition in a community repository (e.g. GitHub). See the Nature Portfolio guidelines for submitting code & software for further information.

Data

Policy information about availability of data

All manuscripts must include a data availability statement. This statement should provide the following information, where applicable:

- Accession codes, unique identifiers, or web links for publicly available datasets
- A description of any restrictions on data availability
- For clinical datasets or third party data, please ensure that the statement adheres to our policy

All single-cell sequencing data are available at GEO (accession number GSE222011). All experimental source data are provided. Per institutional data sharing policies, requests for deidentified individual participant data can be made beginning 12 months after publication and for up to 36 months post-publication. Deidentified individual participant data reported in the manuscript will be shared under the terms of a Data Use Agreement that addresses the privacy and security requirements for safeguarding the data under HIPAA and MSK policies, and may only be used for approved proposals. Requests may be made to balachav@mskcc.org.

Research involving human participants, their data, or biological material

Policy information about studies with human participants or human data. See also policy information about sex, gender (identity/presentation), and sexual orientation and race, ethnicity and racism.

Reporting on sex and gender	The sex of all patients enrolled in the trial is reported in the primary article for this dataset - Rojas et al. Nature 2023 https://www.nature.com/articles/s41586-023-06063-y
Reporting on race, ethnicity, or other socially relevant groupings	The race/ethnicity of all patients enrolled in the trial is reported in the primary article for this dataset - Rojas et al. Nature 2023 https://www.nature.com/articles/s41586-023-06063-y
Population characteristics	Patients were stratified by immune response to autogene cevumeran as described in Methods
Recruitment	Full details of inclusion/enrollment and recruitment are provided in the clinical trial protocol, and the primary article for this dataset - Rojas et al. Nature 2023 https://www.nature.com/articles/s41586-023-06063-y
Ethics oversight	The study was approved by the institutional review board (IRB) at Memorial Sloan Kettering Cancer Center (MSK), the United States Federal Drug Administration (FDA), and was registered on clinicaltrials.gov (NCT04161755). All participants provided written informed consent.

Note that full information on the approval of the study protocol must also be provided in the manuscript.

Field-specific reporting

Please select the one below that is the best fit for your research. If you are not sure, read the appropriate sections before making your selection.

☒ Life sciences ☐ Behavioural & social sciences ☐ Ecological, evolutionary & environmental sciences

For a reference copy of the document with all sections, see nature.com/documents/nr-reporting-summary-flat.pdf

Life sciences study design

All studies must disclose on these points even when the disclosure is negative.

Sample size	For the primary dataset, we targeted to accrue a total of 20 evaluable patients based on estimated sample size needed to evaluate our primary endpoint of safety. Additional details can be found in the primary article – Rojas et al. Nature 2023 https://www.nature.com/articles/s41586-023-06063-y
Data exclusions	No data were excluded.
Replication	All findings were reproducible. All experimental replicates, performed as independent experiments in individual patient samples, are outlined in the figures and figure legends. Technical replicates are also indicated in the figure legends when appropriate.
Randomization	Randomization is not applicable, as the primary study source for this dataset was a single-arm, phase-I clinical trial.
Blinding	In the clinical trial underlying the primary dataset, the investigators were blinded to survival events during immunologic response determination. Other experiments: no blinding, as researches needed access to the sample information to perform the experiments.

Reporting for specific materials, systems and methods

We require information from authors about some types of materials, experimental systems and methods used in many studies. Here, indicate whether each material, system or method listed is relevant to your study. If you are not sure if a list item applies to your research, read the appropriate section before selecting a response.

Materials & experimental systems

n/a	Involved in the study
☐	☒ Antibodies
☐	☒ Eukaryotic cell lines
☒	☐ Palaeontology and archaeology
☒	☐ Animals and other organisms
☐	☒ Clinical data
☒	☐ Dual use research of concern
☒	☐ Plants

Methods

n/a	Involved in the study
☒	☐ ChIP-seq
☐	☒ Flow cytometry
☒	☐ MRI-based neuroimaging

Antibodies

Antibodies used

CD137 - clone 4B4-1, PE (Biolegend Cat# 309804); 3µl/sample
CD3 - clone SK-7, PE-Cy7 (Biolegend Cat# 344816); 4µl/sample
CD4 - clone OKT4, BV650 (Biolegend Cat# 317436); 2 µl/sample
CD45 - clone 2D1, Alexa Fluor 700 (Biolegend Cat# 368514); 5 µl/sample
CD56 - clone HCD56, BV605 (Biolegend Cat# 318334); 2 µl/sample
CD8 - clone SK1, APC-Cy7 (Biolegend Cat# 344714); 2 µl/sample
CD8 - clone SK1, Alexa Fluor 700 (Biolegend Cat# 344724); 2 µl/sample
IFNγ - clone 4S.B3, BV421 (Biolegend Cat# 502532); 5 µl/sample
CD107a - clone H4A3, PE (BD Biosciences Cat# 555801); 20 µl/ sample
CD56 - clone NCAM16.2, BV786 (BD Biosciences Cat# 564058); 5 µl/sample
TNFα - clone MAb11, APC (BD Biosciences Cat# 554514); 2.5 µl/sample
mTCR - clone H57-597, PE-Cy5 (Biolegend Cat #109209), 0.5 µl/sample
HLA-ABC - clone W6/32, APC (Biolegend Cat #311409), 3 µl/sample
DAPI - (BD Biosciences Cat# 564907); 0.2 µl/sample
Fixable viability Dye - eFLuor 520 (Invitrogen Cat# 65-0867-14); 1.0 µl/sample

Validation

All antibodies were validated by the manufacturer and used per their instructions. In our experiments, biological negative controls were included. Additional information on validation can be found on the manufacturer's websites, below.
CD137 - clone 4B4-1, PE (Biolegend Cat# 309804); https://www.biolegend.com/en-ie/products/pe-anti-human-cd137-4-1bb-antibody-1510?GroupID=BLG2203
CD3 - clone SK-7, PE-Cy7 (Biolegend Cat# 344816); https://www.biolegend.com/en-ie/products/pe-cyanine7-anti-human-cd3-antibody-6934
CD4 - clone OKT4, BV650 (Biolegend Cat# 317436); https://www.biolegend.com/en-ie/products/brilliant-violet-650-anti-human-cd4-antibody-7786
CD45 - clone 2D1, Alexa Fluor 700 (Biolegend Cat# 368514); https://www.biolegend.com/en-ie/products/alexa-fluor-700-anti-human-cd45-antibody-12399
CD56 - clone HCD56, BV605 (Biolegend Cat# 318334); https://www.biolegend.com/en-ie/products/brilliant-violet-605-anti-human-cd56-ncam-antibody-7668
CD8 - clone SK1, APC-Cy7 (Biolegend Cat# 344714); https://www.biolegend.com/en-ie/products/apc-cyanine7-anti-human-cd8-antibody-6391

CD8 - clone SK1, Alexa Fluor 700 (Biolegend Cat# 344724); https://www.biolegend.com/en-ie/products/alexa-fluor-700-anti-human-cd8-antibody-9062
IFNγ - clone 4S.B3, BV421 (Biolegend Cat# 502532); https://www.biolegend.com/en-ie/products/brilliant-violet-421-anti-human-ifn-gamma-antibody-7189
CD107a - clone H4A3, PE (BD Biosciences Cat# 555801); https://www.bdbiosciences.com/en-us/products/reagents/flow-cytometry-reagents/research-reagents/single-color-antibodies-ruo/pe-mouse-anti-human-cd107a.555801
CD56 - clone NCAM16.2, BV786 (BD Biosciences Cat# 564058); https://www.bdbiosciences.com/en-us/products/reagents/flow-cytometry-reagents/research-reagents/single-color-antibodies-ruo/bv786-mouse-anti-human-cd56.564058
TNFα - clone MAb11, APC (BD Biosciences Cat# 554514); https://www.bdbiosciences.com/en-us/products/reagents/flow-cytometry-reagents/research-reagents/single-color-antibodies-ruo/apc-mouse-anti-human-tnf.554514
mTCR - clone H57-597, PE-Cy5 (Biolegend Cat #109209) https://www.biolegend.com/de-at/products/pe-cyanine5-anti-mouse-tcr-beta-chain-antibody-273
HLA-ABC - clone W6/32, APC (Biolegend Cat #311409), https://www.biolegend.com/de-at/products/apc-anti-human-hla-a-b-c-antibody-1870
DAPI - (BD Biosciences Cat# 564907); https://www.bdbiosciences.com/en-us/products/reagents/flow-cytometry-reagents/research-reagents/single-color-antibodies-ruo/dapi-solution.564907
Fixable viability Dye - eFLuor 520 (Invitrogen Cat# 65-0867-14); https://www.thermofisher.com/order/catalog/product/65-0867-14

Eukaryotic cell lines

Policy information about cell lines and Sex and Gender in Research

Cell line source(s)	We purified patient peripheral blood mononuclear cells (PBMCs) by density centrifugation over Ficoll-Paque Plus (GE Healthcare) and cultured purified cells in RPMI medium supplemented with 10% fetal bovine serum (FBS, (Nucleus Biologics), 1 mM sodium pyruvate, 2 mM L-glutamine, non-essential amino acids and 2-mercaptoethanol, 100 U ml-1 penicillin-streptomycin (MSK medium preparation core facility), with 100 U ml-1 IL-2 (Peprotech), and 100 U ml-1 IL-15 (Peprotech) added every other day. We purchased pan negative selection purified human T cells (Precision for Medicine). We purchased T2 (174 x CEM.T2) cells (CRL-1992) and K562 cells (CCL-243) from ATCC. 293Vec-RD114 cells (Biovec Pharma) and Phoenix-AMPHO cells (ATCC CRL-3213) were kindly gifted from MSK laboratories.
Authentication	For transduction of T cells, T2 cells, and K562 cells, we authenticated the correct sequence of the retroviral vector by Sanger sequencing before transduction. Then, we validated the generated cell lines by PCR amplification of the inserted transgene and Sanger sequencing. We further validated correct HLA and TCR expression by functional assays with restricted epitopes.
Mycoplasma contamination	PBMCs and donor-derived transduced T cells were not tested for mycoplasma contamination. Cell lines were periodically tested for presence of mycoplasma using the MycoAlert-PlusTM kit (Lonza) at the Antibody and Bioresource Core Facility at MSK.
Commonly misidentified lines (See ICLAC register)	No commonly misidentified lines were used in this study.

Clinical data

Policy information about clinical studies

All manuscripts should comply with the ICMJE guidelines for publication of clinical research and a completed CONSORT checklist must be included with all submissions.

Clinical trial registration	NCT04161755
Study protocol	Study protocol is available (Supplementary File 1).
Data collection	Patients were enrolled from December 2019 to August 2021. Data were collected at MSK during and beyond enrollment period.
Outcomes	Primary endpoint was safety and was assessed using a predefined number of grade 3 adverse events due to atezolizumab and autogene cevumeran per number of patients enrolled (reported in primary article for this dataset – Rojas et al. Nature 2023 https://www.nature.com/articles/s41586-023-06063-y). Secondary endpoints were 18-month recurrence free survival (RFS) and overall survival (OS). We defined recurrence as new lesions by RECIST 1.1, and RFS from either the date of surgery (RFS), or from the date of the last autogene cevumeran priming dose (landmark RFS) to the date of recurrence or death, whichever occurred first. We censored patients without events at the last known date they were recurrence-free. We defined OS from the date of surgery to the date of death. As exploratory endpoints, we measured immune response. Data cut-off was December 1, 2023, extending the median follow-up to 36 months

Plants

Seed stocks

Report on the source of all seed stocks or other plant material used. If applicable, state the seed stock centre and catalogue number. If plant specimens were collected from the field, describe the collection location, date and sampling procedures.

Novel plant genotypes

Describe the methods by which all novel plant genotypes were produced. This includes those generated by transgenic approaches, gene editing, chemical/radiation-based mutagenesis and hybridization. For transgenic lines, describe the transformation method, the number of independent lines analyzed and the generation upon which experiments were performed. For gene-edited lines, describe the editor used, the endogenous sequence targeted for editing, the targeting guide RNA sequence (if applicable) and how the editor was applied.

Authentication

Describe any authentication procedures for each seed stock used or novel genotype generated. Describe any experiments used to assess the effect of a mutation and, where applicable, how potential secondary effects (e.g. second site T-DNA insertions, mosiacism, off-target gene editing) were examined.

Flow Cytometry

Plots

Confirm that:

☒ The axis labels state the marker and fluorochrome used (e.g. CD4-FITC).

☒ The axis scales are clearly visible. Include numbers along axes only for bottom left plot of group (a 'group' is an analysis of identical markers).

☒ All plots are contour plots with outliers or pseudocolor plots.

☒ A numerical value for number of cells or percentage (with statistics) is provided.

Methodology

Sample preparation

We purified patient peripheral blood mononuclear cells (PBMCs) by density centrifugation over Ficoll-Paque Plus (GE Healthcare) and cultured purified cells in RPMI medium supplemented with 10% fetal bovine serum (FBS, (Nucleus Biologics), 1 mM sodium pyruvate, 2 mM L-glutamine, non-essential amino acids and 2-mercaptoethanol, 100 U ml-1 penicillin-streptomycin (MSK medium preparation core facility), with 100 U ml-1 IL-2 (Peprotech), and 100 U ml-1 IL-15 (Peprotech) added every other day.

We stained cells using antibody cocktails in the dark at 4°C, washed, and analyzed. To examine expression of intracellular markers, we surface-stained, fixed, permeabilized, and stained the cells for intracellular proteins using the Fixation and Permeabilization Buffer Kit as per the manufacturer's recommendations (Invitrogen, MA, USA). Full details are provided in the Methods.

Instrument

We analyzed PBMCs, transduction efficiency, and T cell activation, on a FACS LSR Fortessa (BD Biosciences). We sorted T cells using an Aria Cell sorter (BD Biosciences).

Software

Data was analyzed using FACSDiva software (version 8.0.1, BD Bioscience) and FlowJo (version 10).

Cell population abundance

Representative cell abundance is indicated in Figure 4a and Extended Data Figure 9. Due to the scarcity of the samples, we were not able to confirm the purity of the populations within the post-sorting fractions.

Gating strategy

We gated lymphocytes based on size and complexity gating (SSC-A vs FSC-A). We considered events with high SSC-W and FSC-W and normal SSC-H and FSC-H, respectively, as doublets and excluded them from the analysis. We identified dead cells as positive for Fixable Viability Dye 520 or DAPI and excluded them from the analysis. We used the following definitions: human T cells as live, CD45+, CD56-, CD3+ cells; degranulating CD8+ T cells as live, CD56-, CD3+, CD8+, CD107a+; neopeptide-stimulated CD8+ T cells as live, CD56-, CD3+, CD8+, TNF +/IFN +; and activated transduced T cells as live, CD3+, CD8+, mTCR +, 4-1BB+. We set the gates of activation markers using mock-stimulated T cells (DMSO or irrelevant peptides).

☒ Tick this box to confirm that a figure exemplifying the gating strategy is provided in the Supplementary Information.